



**HAL**  
open science

## Potential vorticity diagnostics based on balances between volume integral and boundary conditions

Yves Morel, Jonathan Gula, Aurélien Ponte

► **To cite this version:**

Yves Morel, Jonathan Gula, Aurélien Ponte. Potential vorticity diagnostics based on balances between volume integral and boundary conditions. *Ocean Modelling*, 2019, 138, pp.23-35. 10.1016/j.ocemod.2019.04.004 . hal-02349710

**HAL Id: hal-02349710**

**<https://hal.science/hal-02349710>**

Submitted on 5 Nov 2019

**HAL** is a multi-disciplinary open access archive for the deposit and dissemination of scientific research documents, whether they are published or not. The documents may come from teaching and research institutions in France or abroad, or from public or private research centers.

L'archive ouverte pluridisciplinaire **HAL**, est destinée au dépôt et à la diffusion de documents scientifiques de niveau recherche, publiés ou non, émanant des établissements d'enseignement et de recherche français ou étrangers, des laboratoires publics ou privés.

1 Potential Vorticity diagnostics based on balances between  
2 volume integral and boundary conditions

3 Yves Morel<sup>1,\*</sup>, Jonathan Gula<sup>2,\*</sup>, Aurélien Ponte<sup>2,\*</sup>

---

4 **Abstract**

5 Taking advantage of alternative expressions for potential vorticity (PV) in  
6 divergence forms, we derive balances between volume integral of PV and  
7 boundary conditions, that are then applied to practical computations of PV:

8

- 9 • we propose a new method for diagnosing the Ertel potential vorticity  
10 from model output, that preserves the balances;
- 11 • we show how the expression of PV can be derived in general coordi-  
12 nate systems. This is here emphasised with isopycnic coordinates by  
13 generalising the PV expression to the general Navier-Stokes equations;
- 14 • we propose a generalised derivation for the Haynes-McIntyre imper-  
15 meability theorem, which highlights the role of the bottom boundary  
16 condition choice (e.g. no-slip vs free-slip) and mixing near the bottom  
17 boundary for the volume integral of PV.

18 The implications of balances between volume integral of PV and boundary  
19 conditions are then analysed for specific processes at various scales:

- 20 • at large scale, we show how an integral involving surface observations  
21 (derived from satellite observations) is linked to the integral of PV

---

\*Corresponding author

*Email addresses:* [yves.morel@shom.fr](mailto:yves.morel@shom.fr) (Yves Morel),

[jonathan.gula@univ-brest.fr](mailto:jonathan.gula@univ-brest.fr) (Jonathan Gula), [aurelien.ponte@ifremer.fr](mailto:aurelien.ponte@ifremer.fr)

(Accepted for publication in *Journal of Physical Oceanography*)

April 23, 2019

<sup>1</sup>LEGOS, Université de Toulouse, CNES, CNRS, IRD, UPS, Toulouse 31400, France

<sup>2</sup>LOPS, Université de Brest, CNRS, Ifremer, IRD, IUEM, Brest 29280, France

22 within a layer (between two isopycnals). This surface integral can be  
23 calculated for models and observations and can be used for validation;

24 • at mesoscale or sub-mesoscale, we analyse the relationship between net  
25 PV anomalies and net surface density anomalies for idealised vortices  
26 and 2D fronts. This can help determining vortex or jet structures for  
27 idealised studies or empirical methodologies;

28 • we also confirm and integrate previous results on the modification of  
29 PV within a bottom boundary layer into a single diagnostic taking  
30 into account the effect of density and velocity modifications by dia-  
31 batic processes along the topography and diapycnal mixing within the  
32 boundary layer.

33 *Keywords:* Potential vorticity, boundary conditions, general circulation,  
34 vortex, fronts, boundary layers.

---

## 35 1. Introduction

36 It is well known that Ertel's Potential Vorticity (PV, see Ertel, 1942)  
37 is an important quantity when studying the circulation at all scales in geo-  
38 physical fluids: the conservation property of PV -in adiabatic evolution- and  
39 the inversion principle (the geostrophic velocity field can be inferred from  
40 the PV field and boundary conditions) are key principles to interpret the  
41 ocean dynamics (see Hoskins et al., 1985; McWilliams, 2006, and section 2  
42 for more details). Conservation and inversion of PV are the basis of the  
43 quasigeostrophic (QG) model (Pedlosky, 1987) that has been successfully  
44 used in pioneering studies aiming at understanding and modelling the ocean  
45 circulation from basin gyres (Rhines and Young, 1982a,b; Luyten et al.,

46 1983; Holland et al., 1984; Rhines, 1986; Talley, 1988; Marshall and Nurser,  
47 1992) to current instabilities (Charney and Stern, 1962), geophysical turbu-  
48 lence (McWilliams, 1984) and mesoscale dynamics (McWilliams and Flierl,  
49 1979; Sutyrin and Flierl, 1994).

50 In the QG framework, PV is related to the streamfunction by a linear  
51 elliptic differential operator (Pedlosky, 1987; Cushman-Roisin and Beckers,  
52 2011), which has several important consequences. First, boundary condi-  
53 tions impose important dynamical constraints too. In a QG framework  
54 Bretherton (1966) has shown that surface or bottom outcropping of isopyc-  
55 nic surfaces is dynamically similar to a shallow layer of high PV anomaly (in  
56 practice a Dirac delta sheet), whose strength can be related to the density  
57 anomaly. This has led to the generalised surface quasigeostrophic (SQG)  
58 model (Held et al., 1995; Lapeyre, 2017). Lateral boundaries can be impor-  
59 tant too for the inversion of PV. In the QG or SQG framework, it has been  
60 shown that the velocity field away from a region of PV anomalies decreases  
61 slowly -as the inverse of the distance from the region- unless PV and surface  
62 density satisfy an integral constraint (Morel and McWilliams, 1997; Assassi  
63 et al., 2016). In models, practical inversion of PV, with given surface and  
64 bottom density fields, is often done considering biperiodic domains (Lapeyre  
65 et al., 2006; Wang et al., 2013), which can lead to discrepancies if the latter  
66 constraint is not satisfied.

67 Second, since the relationship between PV and the circulation is linear  
68 at first order (QG and SQG), the balance between smoothed/averaged fields  
69 is preserved, provided averaging is done using a linear convolution.

70 Moreover, PV concept is also useful for forced dissipative dynamics.  
71 For instance, diapycnal mixing does not change the volume integral of PV  
72 within a layer bounded by isopycnic surfaces, which shows that PV can

73 only be diluted or concentrated when the layer respectively gains or loses  
74 mass (Haynes and McIntyre, 1987, 1990). The influence of viscous surface  
75 or bottom stress on the PV evolution has also been analysed theoretically  
76 (Thomas, 2005; Taylor and Ferrari, 2010; Benthuisen and Thomas, 2012,  
77 2013). Thus, the consequences of diabatic effects on the ocean dynamics  
78 can again be analysed and interpreted in terms of PV modification from  
79 basin scales (see for instance Hallberg and Rhines, 1996, 2000; Czaja and  
80 Hausmann, 2009) to meso and submesoscales (see for instance Morel and  
81 McWilliams, 2001; Morel et al., 2006; Morel and Thomas, 2009; Rossi et al.,  
82 2010; Meunier et al., 2010; Thomas et al., 2013; Molemaker et al., 2015;  
83 Gula et al., 2015, 2016, 2019; Vic et al., 2015; Giordani et al., 2017).

84 To conclude, the ocean circulation and PV are linked and calculating PV  
85 at all scales under adiabatic or diabatic conditions is thus of considerable in-  
86 terest for geophysical fluid dynamics. In QG or SQG models, it is possible to  
87 ensure consistent balances between circulation, PV and surface, bottom and  
88 lateral boundary conditions, from local to averaged fields. In more complex  
89 models, PV calculation involves many velocity and density derivatives, in  
90 particular in non-isopycnic models, and keeping the link between averaged  
91 PV and averaged circulation implies to find a consistent calculation of PV.  
92 If several studies have used diagnostics involving PV, they remain rare and  
93 none have discussed the PV calculations in details, in particular to evaluate  
94 if the relationships between PV and boundary conditions are maintained  
95 and if averaging can be done consistently.

96 The Bretherton principle (Bretherton, 1966) has been recently revisited  
97 and extended by Schneider et al. (2003) who generalised the concept of PV  
98 to take into account the dynamical effect of outcropping for the general  
99 Navier Stokes equations. To do so, they used the alternative divergence

100 form for the expression of PV (Vallis, 2006). In this paper, we show how  
 101 this divergence form of PV naturally leads to general constraints on volume  
 102 balances of PV and boundary conditions (section 3). These follow from the  
 103 definition of PV and are independent of the dynamics (adiabatic or diabatic)  
 104 of the flow. In section 4 we show that the divergence form also makes PV  
 105 computations easier and consistent, in the sense that balances are automati-  
 106 cally preserved when integrating PV (a consequence of the divergence form).  
 107 We then propose several frameworks, involving dynamics at different scales,  
 108 to discuss the generalised constraints between PV and surface, bottom or  
 109 lateral boundary conditions (section 5). We summarise and discuss our re-  
 110 sults in the concluding section. Section 2 summarises basic definitions and  
 111 properties of PV which are not new and can be skipped by readers familiar  
 112 with PV.

## 113 **2. Reminders on potential vorticity**

### 114 *2.1. Definition of Ertel potential vorticity*

115 Ertel (1942) defined Potential Vorticity as:

$$\begin{aligned}
 PV_{Ertel} &\equiv -(\vec{\nabla} \times \vec{U} + \vec{f}) \cdot \frac{\vec{\nabla} \rho}{\rho} \\
 &= -(\vec{\nabla} \times \vec{U}_a) \cdot \frac{\vec{\nabla} \rho}{\rho}
 \end{aligned}
 \tag{1}$$

116 where  $\vec{U}$  is the fluid velocity field in the reference frame of the rotating Earth,  
 117  $\rho$  is the potential density (in the ocean and entropy in the atmosphere),  
 118  $\vec{U}_a = \vec{U} + \vec{\Omega} \times \vec{r}$  is the absolute velocity, where  $\vec{\Omega} = (0, \Omega_y, \Omega_z)$  is the  
 119 rotation vector of the Earth,  $\vec{r}$  is the position relative to the Earth center  
 120 and  $\vec{f} = (0, f_y, f_z) = \vec{\nabla} \times (\vec{\Omega} \times \vec{r}) = 2 \vec{\Omega}$  (see Fig. 1). Note that  $\vec{f}$  is

121 fixed but its components in some coordinate system (spherical coordinates  
 122 for instance) can vary with position. The minus sign on the left-hand side of  
 123 (1) is so that PV is generally positive for gravitationally stable - low Rossby  
 124 number flows in the northern hemisphere.

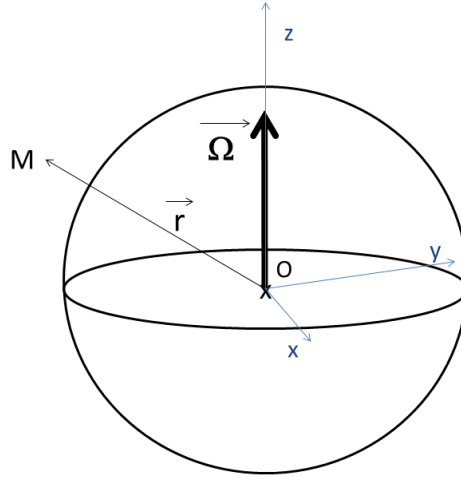


Figure 1: General Earth referential.

125 In the ocean, the Boussinesq approximation is typically valid and  $\vec{\nabla}\rho/\rho$   
 126 can be replaced by  $\vec{\nabla}\rho/\rho_0$ , where  $\rho_0$  is a mean oceanic density.  $\rho_0$  can then  
 127 be omitted from the definition of PV and we can use:

$$\begin{aligned}
 PV_{Ertel} &= -(\vec{\nabla} \times \vec{U} + \vec{f}) \cdot \vec{\nabla}\rho \\
 &= -(\vec{\nabla} \times \vec{U}_a) \cdot \vec{\nabla}\rho
 \end{aligned}
 \tag{2}$$

128 We retain this definition for PV as it leads to clearer expressions for the  
 129 calculations we present and the formulas we obtain. This approximation is

130 however not necessary and all the following results are valid provided  $\rho$  is  
 131 replaced by  $G(\rho) = \log(\rho)$  (see Appendix B).

## 132 2.2. Properties

### 133 2.2.1. Conservation

134 The non-hydrostatic Navier-Stokes equations (with Boussinesq approxi-  
 135 mation) are:

$$\begin{aligned} \frac{d}{dt}\vec{U} + \vec{f} \times \vec{U} &= -\frac{\vec{\nabla}P}{\rho_0} - \vec{g}\frac{\rho}{\rho_0} + \vec{F} \\ \text{div}(\vec{U}) &= 0 \\ \frac{d}{dt}\rho &= \dot{\rho} \end{aligned} \quad (3)$$

136 where  $\vec{U} = (u, v, w)$  is the velocity field,  $\frac{d}{dt}\phi = \partial_t\phi + (\vec{U} \cdot \vec{\nabla})\phi$ ,  $\vec{f} = (0, f_y, f_z)$   
 137 is the Coriolis vector,  $P$  is the pressure,  $\rho$  is the potential density and  
 138  $\vec{F} = (F_x, F_y, F_z)$  and  $\dot{\rho}$  are terms associated with diabatic processes for  
 139 momentum and density fields.

140 The Lagrangian evolution of Ertel PV can be derived from Eq. 3:

$$\frac{d}{dt}PV_{Ertel} = -(\vec{\nabla} \times \vec{F}) \cdot \vec{\nabla}\rho - (\vec{\nabla} \times \vec{U} + \vec{f}) \cdot \vec{\nabla}\rho \quad (4)$$

141 As shown by Ertel (1942),  $PV_{Ertel}$  is thus conserved in regions where diabatic  
 142 processes are negligible.

143 The evolution/conservation of PV following fluid particles is a major  
 144 constraint for geophysical fluid dynamics (Hoskins et al., 1985). To study  
 145 geophysical fluids, simplified forms of Eq. 3 are sought which conserve a sim-  
 146 plified expression for PV (White et al., 2005). This is the case for instance for



147 quasigeostrophic or primitive equations (Pedlosky, 1987; Cushman-Roisin  
 148 and Beckers, 2011; McWilliams, 2006). For the primitive equations, the hy-  
 149 drostatic approximation is assumed and  $f_y$  is neglected, PV can be written  
 150 (White et al., 2005):

$$PV_{PE} = -(\partial_x v - \partial_y u + f_z) \partial_z \rho + \partial_z v \partial_x \rho - \partial_z u \partial_y \rho \quad (5)$$

151 where  $f_z$  is the (local) vertical component of the Coriolis vector and is called  
 152 Coriolis parameter.

153 The Lagrangian conservation of  $PV_{PE}$  is more conveniently derived, and  
 154 achieved in numerical models, using density  $\rho$  instead of the geopotential  
 155 vertical coordinate  $z$ . This has been one of the motivation for the develop-  
 156 ment of isopycnic coordinate ocean models (see for instance Bleck et al.,  
 157 1992; Hallberg, 1997). Using isopycnic coordinate,  $PV_{PE}$  can be written  
 158 (Cushman-Roisin and Beckers, 2011):

$$PV_{PE} = \frac{\zeta + f_z}{h} \quad (6)$$

159 where  $\zeta = (\partial_x v - \partial_y u) |_\rho$  is the relative vorticity, now calculated using  
 160 horizontal velocity components along isopycnic surfaces and  $h = -\partial_\rho z$  is a  
 161 measure of the local stratification. We will see below how the expression of  
 162 PV can be easily derived in isopycnic coordinates for the full Navier-Stokes  
 163 equations (including terms coming from all components of the Coriolis vector  
 164 and non-hydrostatic effects).

### 165 2.2.2. Inversion

166 If (cyclo)geostrophy is assumed, the velocity field and stratification can  
 167 be calculated from the PV and are associated with the balanced dynamics

168 (Hoskins et al., 1985; Davis and Emanuel, 1991; McIntyre and Norton, 2000;  
 169 Morel and McWilliams, 2001; Herbette et al., 2003, 2005). The PV of a fluid  
 170 at rest and with a horizontally homogeneous stratification is not null. The  
 171 potential vorticity anomaly (PVA) is defined as the difference between total  
 172 PV and a reference PV associated with a state of rest of the entire fluid:

$$PVA = PV - \overline{PV}^{rest} \quad (7)$$

173 *PVA* is the part of the PV that is linked to the balanced dynamics and, at  
 174 first order, it corresponds to the quasigeostrophic PV (Davis and Emanuel,  
 175 1991; McIntyre and Norton, 2000; Herbette et al., 2003).

176 The PV of the state at rest is given by the stratification at rest:

$$\overline{PV}^{rest} = -\vec{f} \cdot \vec{\nabla} \bar{\rho} |_{\rho} = -f_z \partial_z \rho |_{\rho} = -\frac{f_z}{\partial_\rho \bar{z}(\rho)} = \frac{f_z}{\bar{h}} \quad (8)$$

177 An important point is that in Eq. 7 PVA has to be calculated along surfaces  
 178 of constant density. This is underlined by the  $|_{\rho}$  symbol in Eq. 8, which is  
 179 valid for both non-hydrostatic and primitive equations. The stratification at  
 180 rest  $\bar{\rho}$  is associated with the adiabatic rearrangement of the density to get a  
 181 horizontally uniform field (Holliday and McIntyre, 1981; Kang and Fringer,  
 182 2010) and it is generally not easy to determine. PVA is thus often used in  
 183 idealised configurations where the fluid is at rest in some area (generally at  
 184 the edge of the domain see sections 5.2 and 5.3 below). Alternatively, PVA  
 185 can be associated with small scale processes, superposed on a larger scale  
 186 circulation. The reference state can then be approximately determined as  
 187 a spatial average (over a distance that is much larger than the processes  
 188 scales).

189 **3. Alternative expressions for PV**

190 *3.1. Divergence form*

191 In the following, the calculations rely on general mathematical properties  
192 relating divergence, curl and gradient of 3D fields and integral properties of  
193 these operators, whose general forms are recalled in Appendix A.

194 Previous studies have shown that Ertel PV, as defined in Eq. 2, can  
195 be expressed in divergence form (see Schneider et al., 2003; Vallis, 2006).  
196 Trivial manipulations (explained in Appendix A, see Eq. A.1) lead to the  
197 following equivalent expressions for the PV in divergence form (remember  
198  $\vec{U}_a = \vec{U} + \vec{\Omega} \times \vec{r}$  is the absolute velocity, see Fig. 1):

$$PV_{Ertel} = -div(\vec{U}_a \times \vec{\nabla}\rho) \quad (9a)$$

$$= -div(\rho (\vec{\nabla} \times \vec{U}_a)) \quad (9b)$$

$$= -div(\vec{U} \times \vec{\nabla}\rho) - div(\rho \vec{f}). \quad (9c)$$

199 Notice that these expressions are exact, whatever the evolution (diabatic or  
200 adiabatic) of PV and have been reported and/or used before, in particular  
201 in atmospheric sciences (see Haynes and McIntyre, 1987; Bretherton and  
202 Schar, 1993; Schneider et al., 2003; Vallis, 2006). Here we demonstrate that  
203 they also lead to consistent and convenient practical approach to calculating  
204 and analysing PV in ocean modelling.

205 *3.2. Implication for the integral of PV*

206 Using Ostrogradsky-Stokes theorem (see Appendix A), the previous di-  
207 vergence form of the PV simplifies the calculation of the integral of  $PV_{Ertel}$

208 over a volume  $V$ . It can be calculated from the knowledge of the den-  
 209 sity, velocity or relative vorticity fields around the surface  $\partial V$  containing  $V$ .  
 210 Equations 9 give the exact expressions:

$$\int \int \int_V PV_{Ertel} dV = - \int \int_{\partial V} \rho (\vec{\nabla} \times \vec{U}_a) \cdot d\vec{S} \quad (10a)$$

$$= - \int \int_{\partial V} (\vec{U}_a \times \vec{\nabla} \rho) \cdot d\vec{S} \quad (10b)$$

$$= - \int \int_{\partial V} \rho \vec{f} \cdot d\vec{S} - \int \int_{\partial V} (\vec{U} \times \vec{\nabla} \rho) \cdot d\vec{S}. \quad (10c)$$

211 The previous expressions follow from the definition of PV and do not depend  
 212 on equations governing its evolution. They represent exact instantaneous  
 213 diagnostics of net PV within a volume and should not be confused with  
 214 the general flux form of the PV evolution equation (Haynes and McIntyre,  
 215 1987).

#### 216 **4. Applications to the calculation of PV**

217 In this section, we discuss how the divergence formulation, and its asso-  
 218 ciated integral constraints Eq. 10, yield an easier way to diagnose PV and  
 219 maintain balances between volume integral of PV and boundary conditions  
 220 (Eq. 10).

##### 221 *4.1. PV diagnostics for numerical models*

222 The diagnosis of PV from numerical model outputs is generally cum-  
 223 bersome if the literal form (Eq. 2 or 5) is chosen as it implies numerous  
 224 gradients calculated at different grid points, which then have to be aver-  
 225 aged. The use of the divergence form simplifies the PV calculation and also  
 226 preserves Eq. 10.

227 As they are used in the majority of ocean circulation models, we consider  
 228 a 3D C-grid, which are 3D extensions of the horizontal Arakawa C-grid (see  
 229 Fig. 2 and Arakawa and Lamb, 1977). Using Cartesian coordinates, we  
 230 start from the divergence form of PV (9b) rewritten as:

$$\begin{aligned}
 PV_{Ertel} &= -div(\rho (\vec{\zeta} + \vec{f})) \\
 &= -\partial_x(\rho(\zeta^x + f^x)) - \partial_y(\rho(\zeta^y + f^y)) - \partial_z(\rho(\zeta^z + f^z)) \quad (11)
 \end{aligned}$$

231 where  $\vec{\zeta} = \vec{\nabla} \times \vec{U}$  and:

$$\begin{aligned}
 \zeta^x &= \partial_y w - \partial_z v \\
 \zeta^y &= -\partial_x w + \partial_z u \\
 \zeta^z &= \partial_x v - \partial_y u. \quad (12)
 \end{aligned}$$

232 The elementary cell for which PV is calculated has the density values  
 233 at its corners (see Fig. 2). As is clear from Fig. 2,  $\zeta^z$  values need to  
 234 be calculated at the center of lower and upper sides of the cell. It can be  
 235 calculated using the circulation along edges of the cell lower and upper sides.  
 236 An interesting property of 3D C-grid is that this is straightforward, thanks  
 237 to the position of the velocity points (located at the middle of edges parallel  
 238 to the velocity component). Density is averaged over the 4 density points  
 239 located at the side corners. The same calculation is also valid for the other  
 240 sides of the cell.

241 As a result, the PV of the cell can easily be calculated from physical  
 242 fields within this single cell. We get:

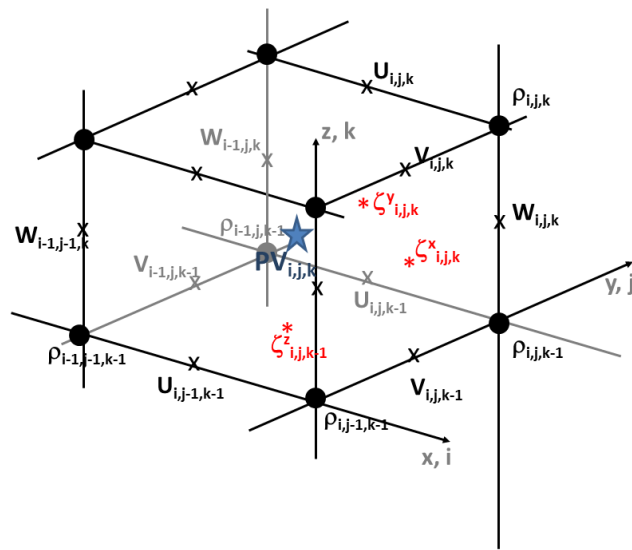


Figure 2: Elementary cell, for a 3D C-grid, used for the calculation of PV. We consider Cartesian coordinates  $(x, y, z)$  associated with indices  $(i, j, k)$ .

$$\begin{aligned}
\zeta_{i,j,k}^x &= \frac{w_{i,j,k} - w_{i,j-1,k}}{\Delta y} - \frac{v_{i,j,k} - v_{i,j,k-1}}{\Delta z} \\
\zeta_{i,j,k}^y &= -\frac{w_{i,j,k} - w_{i-1,j,k}}{\Delta y} + \frac{u_{i,j,k} - u_{i,j,k-1}}{\Delta z} \\
\zeta_{i,j,k}^z &= \frac{v_{i,j,k} - v_{i-1,j,k}}{\Delta x} - \frac{u_{i,j,k} - u_{i,j-1,k}}{\Delta y},
\end{aligned} \tag{13}$$

243 and finally

$$\begin{aligned}
PV_{i,j,k} &= -\frac{\overline{\rho^x}_{i,j,k}(\zeta_{i,j,k}^x + f_{i,j,k}^x) - \overline{\rho^x}_{i-1,j,k}(\zeta_{i-1,j,k}^x + f_{i-1,j,k}^x)}{\Delta x} \\
&\quad -\frac{\overline{\rho^y}_{i,j,k}(\zeta_{i,j,k}^y + f_{i,j,k}^y) - \overline{\rho^y}_{i,j-1,k}(\zeta_{i,j-1,k}^y + f_{i,j-1,k}^y)}{\Delta y} \\
&\quad -\frac{\overline{\rho^z}_{i,j,k}(\zeta_{i,j,k}^z + f_{i,j,k}^z) - \overline{\rho^z}_{i,j,k-1}(\zeta_{i,j,k-1}^z + f_{i,j,k-1}^z)}{\Delta z},
\end{aligned} \tag{14}$$

244 where

$$\overline{\rho^x}_{i,j,k} = 1/4(\rho_{i,j,k} + \rho_{i,j,k-1} + \rho_{i,j-1,k} + \rho_{i,j-1,k-1}) \tag{15}$$

245 is the density calculated at the position of  $\zeta_{i,j,k}^x$  (see Fig. 2), and so forth for  
246 the other components. The Coriolis components  $f_{i,j,k}^{x/y/z}$  are calculated at the  
247 location of the  $\zeta_{i,j,k}^{x/y/z}$  points. Note that for the specific discretization of the  
248 3D C-grid (see Fig. 2), the divergence form leads to a compact expression  
249 of PV : in Eq. 14 PV is calculated using density and velocity values from a  
250 single grid cell.

251 Equation 14 has a flux form, which ensures that, given a volume  $V$ ,  
252 the integral of PV calculated over  $V$  using the accumulation of individual  
253 cells or using Eq. 10 exactly match, thus preserving the general balances  
254 between integral of PV and boundary conditions for any volume. Flux form

255 PV expressions can be derived for B-grids or other grids, with a similar  
 256 property.

257 *4.2. General PV expression in isopycnal coordinates*

258 The integral constraints 10 may be used for an easier derivation of the  
 259 expression of PV in any coordinate systems and for the full Navier-Stokes  
 260 equations. As an example, we calculate PV using the isopycnic coordinate  
 261  $\rho$  instead of the geopotential coordinate  $z$  (see section 4a of Schneider et al.,  
 262 2003). This is of interest as the interpretation of the PV evolution, in  
 263 particular the PV anomaly, has to be made along isopycnic surfaces (Hoskins  
 264 et al., 1985).

265 For the sake of simplicity, we just replace the vertical Cartesian coordi-  
 266 nate  $z$  by  $\rho$  and we keep the Cartesian  $(x, y)$  coordinates in the horizontal  
 267 (see Fig. 3). Other systems (for instance spherical) can be used without  
 268 much more complications. We also keep the orthogonal Cartesian elemen-  
 269 tary vectors  $(\vec{i}, \vec{j}, \vec{k})$  associated with axis  $(Ox, Oy, Oz)$  (see Fig. 3) to express  
 270 all vectors.

271 In this framework,  $z = z(x, y, \rho)$  is the vertical position of isopycnic  
 272 surfaces, and to calculate PV, we will use Eq. 10b, which only requires the  
 273 evaluation of the density gradient  $\vec{\nabla}\rho = \partial_x\rho \vec{i} + \partial_y\rho \vec{j} + \partial_z\rho \vec{k}$ , but using the  
 274  $(x, y, \rho)$  coordinates. To do so, we use:

$$\begin{aligned}
 h &= -\partial_\rho z = -1/\partial_z \rho \\
 \partial_x z |_{y,\rho} &= -h \partial_x \rho |_{y,z} \\
 \partial_y z |_{x,\rho} &= -h \partial_y \rho |_{x,z}
 \end{aligned}$$

275 The density gradient is then given by:



$$\vec{\nabla}\rho = \frac{1}{h}[\partial_x z \vec{i} + \partial_y z \vec{j} - \vec{k}] \quad (16)$$

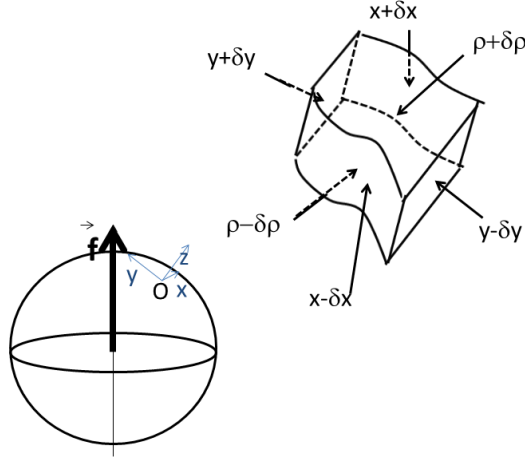


Figure 3: Coordinate system  $(x, y, \rho)$  and elementary volume and surfaces used to calculate  $PV_{Ertel}$  using the isopycnic coordinate.

276 Equation 10b is then applied to an elementary volume bounded by two  
277 isopycnic surfaces sketched in Fig. 3:

$$\begin{aligned} \int \int \int_{\delta V} PV_{Ertel} dV &= - \int \int_{\partial \delta V} (\vec{U}_a \times \vec{\nabla}\rho) \cdot d\vec{S} \\ &= - [(\vec{U}_a \times \vec{\nabla}\rho) \cdot d\vec{S}]_{\partial \delta V} \end{aligned} \quad (17)$$

278 where  $[\cdot]_{\partial \delta V}$  is the flux through all surfaces delimiting  $\delta V$ . Note that  $\vec{U}_a =$   
279  $u_a \vec{i} + v_a \vec{j} + w_a \vec{k}$  remains the absolute velocity field expressed in the  
280 orthogonal Cartesian system.

281 Since the flux across isopycnic surfaces ( $\rho \pm \delta\rho$ ) is null and since the other  
 282 surfaces are simple (vertical planes of constant  $y$  or  $x$ ), Eq. 17 gives:

$$\begin{aligned}
 PV_{Ertel}^\rho \delta V = & - [(\vec{U}_a \times \vec{\nabla}\rho) \cdot \vec{i} \, 2\delta y \, 2h\delta\rho]_{x-\delta x}^{x+\delta x} \\
 & - [(\vec{U}_a \times \vec{\nabla}\rho) \cdot \vec{j} \, 2\delta x \, 2h\delta\rho]_{y-\delta y}^{y+\delta y}
 \end{aligned} \quad (18)$$

283 Given that  $\delta V = 2\delta x \, 2\delta y \, 2\delta z = -2\delta x \, 2\delta y \, 2h\delta\rho$  and

$$\vec{U}_a \times \vec{\nabla}\rho = -\frac{1}{h}(v_a + w_a\partial_y z, -u_a - w_a\partial_x z, -u_a\partial_y z + v_a\partial_x z) \quad (19)$$

284 Eq. 18 gives:

$$\begin{aligned}
 PV_{Ertel}^\rho &= \frac{\partial_x(v_a + w_a\partial_y z) |_\rho - \partial_y(u_a + w_a\partial_x z) |_\rho}{h} \\
 &= \frac{\partial_x(v + w\partial_y z) |_\rho - \partial_y(u + w\partial_x z) |_\rho + f_z - f_y\partial_y z}{h}
 \end{aligned} \quad (20)$$

285 which is a generalised form of Eq. 6 with additional terms (in particular all  
 286 components of the Coriolis effect). The terms  $(u + w\partial_x z) |_\rho$ ,  $(v + w\partial_y z) |_\rho$   
 287 represent the projection of the velocity field on the plane tangent to the  
 288 isopycnic surface.

289 This exact general result can also be derived using Eq. 2, with a change  
 290 of coordinate. But the calculations based on Eq. 10 offer a straightforward  
 291 method.

#### 292 4.3. Integration of PV in a "layer"

293 We consider a volume  $V$  constituted of a "layer" embedded between  
 294 two isopycnic surfaces associated with densities  $\rho_1$  and  $\rho_2$ , that can outcrop  
 295 at the surface or bottom (see Fig. 4). The total PV contained within  $V$

296 may be deduced from Eq. 10c and trivial calculations (taking advantage  
 297 of the fact that the boundaries  $\partial V$  of the layer are partly delimited by  
 298 isentropic/isopycnic surfaces, and some rearrangements using Eq. A.4).

299 This leads to the following form, which depends only on physical fields  
 300 at the surface and bottom outcropping regions:

$$\begin{aligned}
 \int \int \int_V PV_{Ertel} dV = & - \int \int_{S^s+S^b+S^w} (\vec{U} \times \vec{\nabla}\rho) \cdot d\vec{S} \\
 + [ \int \int_{S^s} (\rho_1 - \rho_s) d\vec{S} & + \int \int_{S^b+S^w} (\rho_1 - \rho_b) d\vec{S} + \int \int_{S^{\rho_2}} (\rho_1 - \rho_2) d\vec{S} ] \cdot \vec{f}
 \end{aligned} \tag{21}$$

301 where  $\rho_s(x, y)$  is the density at the ocean surface and  $\rho_b(x, y)$  the density  
 302 along the bottom of the ocean. This form takes advantage of the expression  
 303 Eq. 10c to deal with volumes delimited by the two isopycnic surfaces  $S^{\rho_1}$  and  
 304  $S^{\rho_2}$ . Part of the layer boundaries are however associated with outcropping  
 305 surfaces where density varies ( $S^s$ ,  $S^w$  and  $S^b$  see Fig. 4). The first right  
 306 hand side term of Eq. 21 depends on  $\vec{U} \times \vec{\nabla}\rho$  and has to be evaluated along  
 307 these surfaces. For this term, depending on the boundary condition used,  
 308 it may be more convenient to switch back to a form in  $\rho \vec{\zeta}$  like in Eq. 10a.  
 309 This has to be done carefully using Eq. A.4 (see Appendix A). For instance  
 310 we obtain for the surface  $S^s$ :

$$- \int \int_{S^s} (\vec{U} \times \vec{\nabla}\rho) \cdot d\vec{S} = \int \int_{S^s} (\rho_1 - \rho_s) \zeta_s dx dy \tag{22}$$

311 Finally, notice that the bottom surface has been divided in "Sidewalls" and  
 312 "Bottom" regions ( $S^w$  and  $S^b$ , see Fig. 4), possibly associated with different  
 313 boundary conditions. This is artificial if both surfaces are associated with

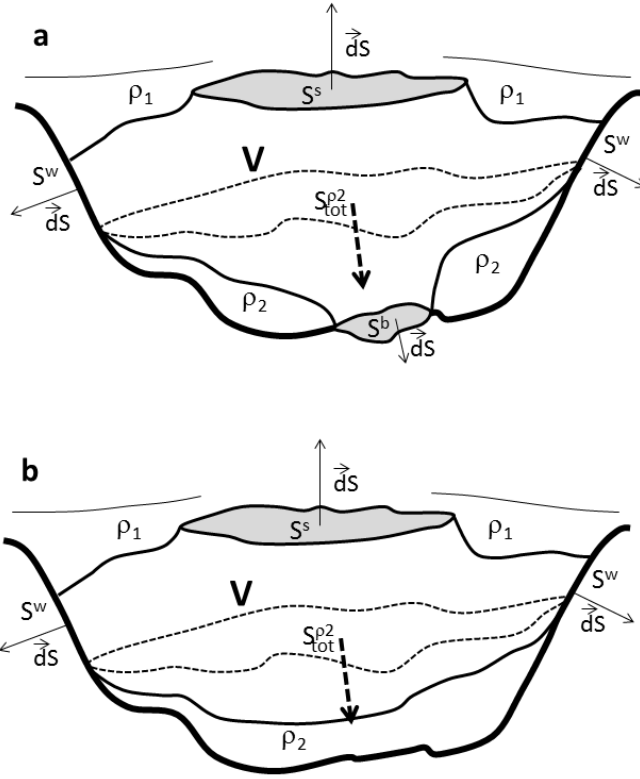


Figure 4: General shape of a layer, bounded by two isopycnic surfaces  $S^{\rho_1}$  and  $S^{\rho_2}$ , determining a volume where we integrate  $PV$ . Outcropping may occur at the surface ( $S^s$ ) and at the bottom ( $S^b$ ). As sketched in the upper plot (a) "Sidewalls" ( $S^w$ ) and "Bottom" ( $S^b$ ) surfaces are sometimes distinguished in numerical model. In this case, layers outcropping at the surface and sidewalls can have special constraints (b), as discussed in section 4.4.

314 the seafloor but we did make a difference for the sake of generality. For  
 315 instance in academic configurations, such as a rectangular basin, boundary  
 316 conditions at the walls and at the bottom can differ.

#### 317 4.4. Impermeability theorem

318 The impermeability theorem (Haynes and McIntyre, 1987, 1990) states  
 319 that there is no net transport of PV across isopycnic (or isentropic) surfaces,  
 320 whatever the evolution. As already shown by Vallis (2006), Eq. 10b is a  
 321 straightforward demonstration of this theorem. Indeed, across such surfaces,  
 322  $d\vec{S}$  is parallel to  $\vec{\nabla}\rho$  and Eq. 10b shows that they do not contribute to the  
 323 calculation of the PV volume integral, whatever the evolution of the isopy-  
 324 cnic surfaces. Thus, if there are no outcropping regions and the isopycnic  
 325 surfaces are closed, the volume integral of Ertel PV within closed isopycnic  
 326 surfaces is and remains null, whatever the evolution. Alternatively, modi-  
 327 fication of the volume integral of PV in an isopycnic layer is only possible  
 328 when isopycnic surfaces outcrop (Haynes and McIntyre, 1987).

329 This principle can be slightly extended. Considering a layer without  
 330 surface outcropping, and considering a no-slip boundary condition at the  
 331 ocean bottom ( $\vec{U}^w = \vec{U}^b = \vec{0}$ ), Eq. 21 gives:

$$\int \int \int_V PV_{Ertel} dV = \left[ \int \int_{S^b+S^w} (\rho_1 - \rho_b) d\vec{S} + \int \int_{S^{\rho_2}} (\rho_1 - \rho_2) d\vec{S} \right] \cdot \vec{f}. \quad (23)$$

332 If  $\vec{U}^w = \vec{U}^b = \vec{0}$ , the density distribution along the bottom can only be  
 333 modified by diabatic (mixing) effects along the bottom. If the latter are  
 334 negligible, the density field along the bottom is constant, and Eq. 23 then  
 335 shows that there is no modification of the volume integral of PV. Indeed, in

336 this case, both terms in the right hand side of Eq. 23 are constant. This  
 337 is obvious for the first term. The second term is simply the scalar product  
 338 of  $\vec{f}$  (constant) and the net  $S^{\rho_2}$  surface vector. The latter only depends on  
 339 the position of the edge of the surface, defined by the  $\rho_2$  contour along the  
 340 bottom, and thus constant too (an alternative way to demonstrate this is to  
 341 transform the second term using Eq. A.4, see Appendix A). To conclude,  
 342 with no-slip boundary conditions, the volume integral of PV is only modified  
 343 if there exists mixing of the density near the bottom. In practice, the free-  
 344 slip boundary condition is often preferred in ocean circulation models, the  
 345 implication for the generation of PV will be discussed below (section 5.4).

346 Another case of interest is when outcropping only occurs at the surface  
 347 and sidewalls (Fig. 4 b). In numerical models, sidewalls are sometimes  
 348 considered vertical and the  $f_y$  component of the Coriolis vector is also ne-  
 349 glected, so that  $\vec{f} \cdot d\vec{S} = 0$ . If no-slip boundary conditions are used, many  
 350 terms disappear in Eq. 21 and we then obtain:

$$\int \int \int_V PV_{Ertel} dV = - \int \int_{S^s} (\vec{U} \times \vec{\nabla} \rho) d\vec{S} + \int \int_{S^s} f_z (\rho_1 - \rho_s) dS \quad (24)$$

351 This draws attention to the potential importance of sloping boundaries and  
 352 the  $f_y$  component for the volume integral of PV at basin scale. It also  
 353 shows that the surface terms in Eq. 24 are of special interest and we further  
 354 evaluate their contributions in the next section.

## 355 5. Applications to specific balances

356 As discussed in the introduction, there exists a strong link between ocean  
 357 circulation and the PV field, from mesoscale eddies to large scale currents.  
 358 Equation 21 shows that there exists a balance between a volume integral

359 of PV and boundary conditions. Using the divergence form of PV and the  
360 local PV calculation discussed in section 4.1 allows to preserve this balance.  
361 This is important for the physical interpretation of model outputs in terms  
362 of PV.

363 In this section, we illustrate how the balance can be used at several scales  
364 and for various processes in realistic or idealised configurations, for which  
365 some terms in Eq. 21 can be easily evaluated from observations (e.g. the  
366 surface ones), simplified or neglected (e.g. for no slip boundary conditions).

367 In section 5.1 we discuss how time variations of large scale volume inte-  
368 gral of PV can be related to surface fields for both models and observations.

369 At mesoscale, surface density anomalies play a role similar to PVA  
370 (Bretherton, 1966). In sections 5.2 and 5.3 we show how Eq. 21 can be  
371 applied to isolated vortices and jets. We show that the balance leads to a  
372 precise relationship between surface density anomalies and PVA integrals,  
373 which has to be satisfied for isolated vortices and jets.

374 Finally, in section 5.4 we show how Eq. 21 can be applied to study the  
375 modification of PV in the bottom boundary layer, underlining the strong  
376 impact of the boundary conditions (free/no-slip).

### 377 *5.1. Surface outcropping regions as indicators of the circulation of deep lay-* 378 *ers*

379 For some choices of boundary conditions Eq. 21 reduces to Eq. 24. In  
380 addition, PV can be quickly modified by diabatic processes at the surface  
381 (Thomas, 2005; Morel et al., 2006; Thomas and Ferrari, 2008; Thomas et al.,  
382 2013; Wenegrat et al., 2018). We can thus hypothesise that the surface term:

$$I_{surf} = \int \int_{S^s} [(\rho_1 - \rho_s) \vec{f} - (\vec{U} \times \vec{\nabla} \rho_s)] \cdot d\vec{S}$$

383 dominates the time evolutions of the integral of PV within a deeper layer,  
 384 which is itself linked to modification of the circulation (Rhines and Young,  
 385 1982a,b; Luyten et al., 1983; Holland et al., 1984; Rhines, 1986; Thomas and  
 386 Rhines, 2002; Polton and Marshall, 2003; Deremble et al., 2014). Comparing  
 387  $I_{surf}$  from numerical models and observations is thus of interest.

388 Using  $d\vec{S} = \vec{k} dx dy$  (where  $\vec{k}$  is the vertical elementary vector),  $I_{surf}$  can  
 389 be rewritten:

$$I_{surf} = \int \int_{S^s} [(\rho_1 - \rho_s) \vec{f} - (\vec{U} \times \vec{\nabla} \rho_s)] \cdot \vec{k} dx dy \quad (25)$$

390 Note that the integral in Eq. 25 only requires the knowledge of surface  
 391 fields, in particular  $(\vec{U} \times \vec{\nabla} \rho_s) \cdot \vec{k}$  only depends on the horizontal gradient of  
 392 the surface density.  $I_{surf}$  can be calculated directly for numerical models.  
 393 For observations, satellite observations (possibly complemented by in situ  
 394 surface drifter observations) provide good estimates of the surface circulation  
 395 over most of the ocean down to scales of order 25 km (see for instance Sudre  
 396 and Morrow, 2008; Abernathey and Marshall, 2013; Rio et al., 2014). To do  
 397 so, the surface current is split into a geostrophic component and a component  
 398 induced by the wind stress:

$$\vec{U}_s = \vec{U}_{geo} + \vec{U}_\tau \quad (26)$$

399 The geostrophic component  $\vec{U}_{geo}$  and the associated relative vorticity can  
 400 be calculated from the knowledge of the sea surface height (SSH) observed  
 401 by satellite altimetry:



$$\vec{U}_{geo} = \frac{g}{f_z} \vec{k} \times \vec{\nabla} SSH \quad (27)$$

402 The wind induced surface current can be evaluated from satellite scat-  
 403 terometer observations and using the wind induced Ekman spiral which gives  
 404 (see Cushman-Roisin and Beckers, 2011):

$$\vec{U}_\tau = \frac{\vec{\tau}_w^{-\pi/4}}{\sqrt{f_z \nu}} \quad (28)$$

405 where  $\nu$  is the turbulent eddy viscosity and

$$\vec{\tau}_w^{-\pi/4} = \frac{\rho_a}{\rho_o} C_D \|W\| \vec{W}^{-\pi/4} \quad (29)$$

406 where  $\vec{W}^{-\pi/4}$  is the surface wind but whose orientation has been rotated by  
 407  $-\pi/4$ ,  $\rho_a/\rho_o$  is the ratio of the air to ocean density and  $C_D \simeq 3.10^{-3}$  is the  
 408 turbulent transfer parameter. As a result, the surface term contributing to  
 409 the calculation of the observed PV within a layer (Eq. 25) can be written:

$$I_{surf} = \int \int_{S^s} (\rho_1 - \rho_s) f_z - \left[ \left( \frac{g}{f_z} \vec{k} \times \vec{\nabla} SSH + \frac{\rho_a C_D \|W\| \vec{W}^{-\pi/4}}{\rho_o \sqrt{f_z \nu}} \right) \times \vec{\nabla} \rho_s \right] \cdot \vec{k} \, dx dy \quad (30)$$

410 and can be calculated from the observed sea surface density (calculated using  
 411 SSS and SST from SMOS, Aquarius and microwave satellite observations),  
 412 SSH and surface wind (all fields generally available over most of the ocean at  
 413  $1/4^\circ$  resolution). We believe the comparison of  $I_{surf}$  from numerical models  
 414 (Eq. 25) and from observations (Eq. 30) can provide an interesting new  
 415 diagnostic for the validation of global or basin scale numerical models.

416 *5.2. Constraints for coherent isolated vortices*

417 Most observed eddies in the ocean are isolated<sup>3</sup> (Chelton et al., 2011).  
 418 In QG and SQG models, for coherent isolated vortices, the volume integral  
 419 of PVA and surface density field are linked (Morel and McWilliams, 1997;  
 420 Assassi et al., 2016). We here extend this balance to Ertel PVA.

421 Consider a flat earth for which  $\vec{f} = (0, 0, f_z)$  (f-plane approximation)  
 422 and an axisymmetric vortex over a flat bottom (see Fig. 5 b-d). For the  
 423 sake of simplicity, we also hypothesise that  $\rho$  is constant at the bottom and  
 424 that  $\overline{PV}^{rest}$  is spatially uniform (linear stratification at rest).

425 Integrating the PVA over the control volume  $V_o$  (see Fig. 5 b-d) gives:

$$\begin{aligned}
 \int \int \int_{V_o} PVA \, dV &= \int \int \int_{V_o} (PV_{Ertel} - \overline{PV}^{rest}) \, dV \\
 &= \int \int \int_{V_o} (-\vec{f} \cdot \vec{\nabla} \rho - \overline{PV}^{rest}) \, dV \\
 &\quad + \int \int \int_{V_o} -(\vec{\nabla} \times \vec{U}) \cdot \vec{\nabla} \rho \, dV \tag{31}
 \end{aligned}$$

426 By using that  $\overline{PV}^{rest} = -f_z(\rho_s^\infty - \rho_b)/H$ , Eq. A.1b and the fact that the  
 427 vortex is isolated, we get:

$$\int \int \int_{V_o} (-\vec{f} \cdot \vec{\nabla} \rho - \overline{PV}^{rest}) \, dV = - \int \int_{S^s} (\rho_s - \rho_s^\infty) f_z \, dx \, dy \tag{32}$$

428 and

---

<sup>3</sup>An isolated vortex has a velocity field that decreases more rapidly than  $1/r$ , where  $r$  is the distance from its center, and the horizontal integral of its vorticity is null at any level.

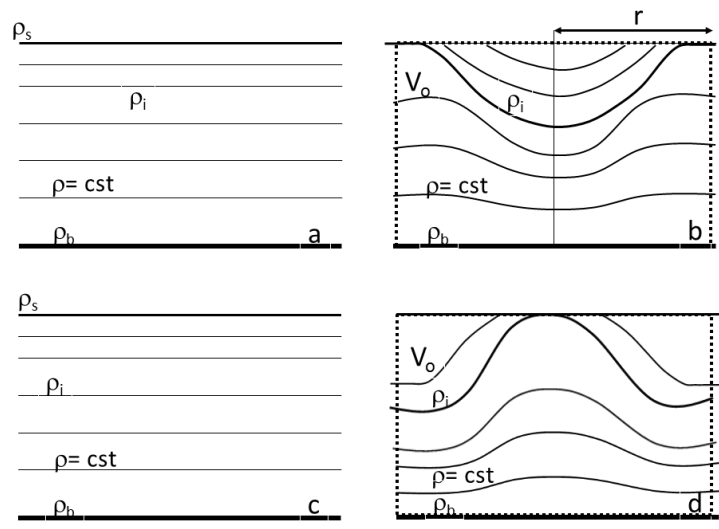


Figure 5: Vertical density structures for axisymmetric vortices having negative (b) and positive (d) surface anomalies.  $V_o$  (dashed contour) is the volume of integration and  $r$  is the distance from the vortex center. The background stratification at rest is indicated in panels a and c.

$$\begin{aligned}
\int \int \int_{V_o} -(\vec{\nabla} \times \vec{U}) \cdot \vec{\nabla} \rho \, dV &= - \int \int_{\partial V_o} \rho (\vec{\nabla} \times \vec{U}) \cdot d\vec{S} \\
&= - \int \int_{S^s} \rho_s \zeta_{surf} \, dx \, dy + O\left(\frac{1}{r}\right) \\
&= - \int \int_{S^s} (\rho_s - \rho_s^\infty) \zeta_{surf} \, dx \, dy + O\left(\frac{1}{r}\right) \quad (33)
\end{aligned}$$

429 where  $\zeta_{surf} = \partial_x v - \partial_y u$  is the relative vorticity at the surface,  $\rho_s^\infty$  is the  
430 surface density at rest or the surface density far from the vortex center, and  
431  $(\rho_s - \rho_s^\infty)$  is the surface density anomaly associated with the vortex<sup>4</sup>.

432 Integration of Eq. 31 over the whole (infinite) domain shows that PV  
433 anomalies associated with isolated vortices have to satisfy:

$$\int \int \int PVA \, dV + \int \int_{S^s} (\rho_s - \rho_s^\infty) (\zeta_{surf} + f_z) \, dx \, dy = 0 \quad (34)$$

434 This extends the integral constraints found in Assassi et al. (2016), which is  
435 modified for strong surface vorticity (when  $|\zeta_{surf}| \simeq f_z$ )<sup>5</sup>. This is the case  
436 for submesoscale vortices (Lapeyre et al., 2006; Klein et al., 2008; Capet  
437 et al., 2008; Roulet et al., 2012; Gula et al., 2015; Molemaker et al., 2015;  
438 Capet et al., 2016).

---

<sup>4</sup>In Eq. 33, the last line is obtained since  $\int \int_{S^s} \zeta \, dx \, dy = 0$  for isolated vortices. The  $O(1/r)$  term accounts for the integration over the bottom and lateral boundaries (dashed contours in Fig. 5). In particular, the lateral contribution scales as  $|\rho H 2\pi r \partial_z U(r)| \leq O(1/r)$ . The  $O(1/r)$  rate of decrease is symbolic and the term simply indicates that these contributions vanish when  $r \rightarrow \infty$ .

<sup>5</sup>Strictly speaking, strong anticyclonic vortices, for which  $\zeta_{surf} < -f_z$ , could even reverse the sign of the deep PVA, but these structures are subject to inertial instability and are not long lived structures.

439 Thus, for isolated vortices, a positive surface density anomaly is accom-  
440 panied with negative PVA. A positive surface density is equivalent to a  
441 positive Dirac delta sheet of PVA (Bretherton, 1966). A similar constraint  
442 holds for a negative density anomaly. Hence, the generalised PVA structure  
443 of isolated vortices has both positive and negative values, which implies op-  
444 posite sign PV gradient and opens the possibility of barotropic/baroclinic  
445 instabilities (Charney and Stern, 1962; Ripa, 1991). This has an impact  
446 on the evolution (stability and displacement) of the vortex (see Morel and  
447 McWilliams, 1997). In idealised studies dealing with the dynamics of iso-  
448 lated vortices, instability of the initial vortex structure can spoil the analysis  
449 and it is preferential to use specific methods, based on the inversion of stable  
450 PV structures, to initialise isolated vortices in models (see Herbette et al.,  
451 2003).

452 Moreover, the constraint Eq. 34 can have implications for methodologies  
453 deriving velocity fields of vortices from surface density observations. The  
454 methodologies empirically generate PVA distributions based on large-scale  
455 PV distributions or statistical correlations between surface density obser-  
456 vations and PVA (Lapeyre et al., 2006; Lapeyre and Klein, 2006; Lapeyre,  
457 2009; Ponte et al., 2013; Wang et al., 2013; Fresnay et al., 2018). In general,  
458 the derived PVA distributions do not satisfy constraint 34. The consequence  
459 is that the velocity field of a reconstructed vortex decreases slowly, which  
460 can lead to spurious calculations near lateral boundaries (the methodolo-  
461 gies often consider periodic boundary conditions). It could be interesting  
462 to modify the methodologies so as to satisfy Eq. 34 in the vicinity of each  
463 vortex. We however have no clue on the spatial distribution of the PVA  
464 from the constraint (PVA poles, crown, vertically aligned or not, vertical  
465 position within the water column, possibly multiple poles of opposite sign,

466 ...) and the reconstruction of the vertical vortex PVA have thus to be done  
 467 carefully.

### 468 5.3. Constraints for jets and surface fronts

469 Similar constraints can be found for density fronts associated with jet-  
 470 like currents. We consider a 2D configuration with no variation in the  $y$   
 471 direction. In 2D, Eq. 10 becomes

$$\begin{aligned}
 \int \int_S PV_{Ertel} dS &= - \int_{\partial S} \rho (\vec{\nabla} \times \vec{U}_a) \cdot \vec{n} dl \\
 &= - \int_{\partial S} (\vec{U}_a \times \vec{\nabla} \rho) \cdot \vec{n} dl \\
 &= - \int_{\partial S} \rho \vec{f} \cdot \vec{n} dl - \int_{\partial S} (\vec{U} \times \vec{\nabla} \rho) \cdot \vec{n} dl \quad (35)
 \end{aligned}$$

472 Consider a 2D front outcropping at the surface but with a constant density  
 473 along a flat bottom (see Fig. 6). The velocity field can be written  $\vec{U} =$   
 474  $\mathcal{V}(x, z) \vec{j}$ , where  $\mathcal{V}$  is the velocity component along the  $y$  axis. For jet-like  
 475 currents the velocity vanishes away from the front:  $\mathcal{V}(x \rightarrow \pm\infty, z) = 0$ .  
 476 The stratification is different on both sides of the front and varies from  
 477  $\bar{\rho}^{-\infty}(z)$  to  $\bar{\rho}^{+\infty}(z)$ .

478 For this configuration, the determination of the reference PV, associated  
 479 with the state at rest, is slightly more delicate, as we hypothesised that both  
 480 the left and right edges of the front are at rest. It has however to be chosen at  
 481 the left edge as only this side covers the entire density range. The reference  
 482 PV is thus  $PV_{rest}^{-\infty}$  and we then integrate PVA from  $x = -\infty$  to  $x = L$ .  
 483 Again, for the sake of simplification, we hypothesise that  $\vec{f} = (0, 0, f_z)$  and  
 484  $PV_{rest}^{-\infty}$  is spatially uniform. Trivial manipulations yield an equation similar  
 485 to Eq. 33:

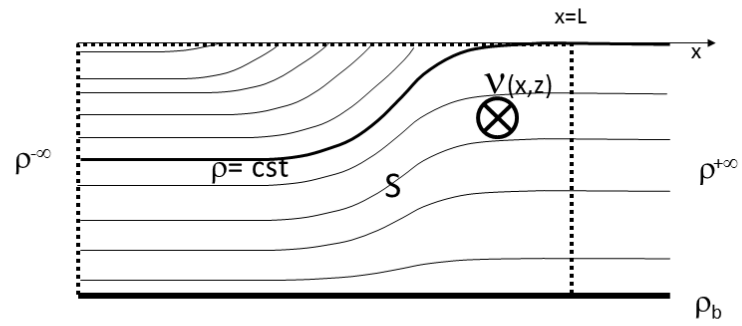


Figure 6: Vertical density structures for a surface outcropping front.  $S$  (dashed contour) is the surface of integration from  $x = -\infty$  to  $x = L$ .

$$\begin{aligned}
\int \int_S PVA \, dS &= \int \int_S PV_{Ertel} - PV_{rest}^{-\infty} \, dS \\
&= - \int_{-\infty}^{x=L} (\rho - \rho^{-\infty})|_{z=0} (\zeta_z + f_z)|_{z=0} \, dx \\
&\quad + \int_{z=-H}^{z=0} (\partial_z \rho \mathcal{V})|_{x=L} \, dz
\end{aligned} \tag{36}$$

486 Assuming the velocity has a jet-like structure,  $\mathcal{V}(x = L, z)$  becomes small  
487 enough so that the last term in Eq. 36, can be neglected. Given the density  
488 structure discussed here (see Fig. 6),  $(\rho - \rho^{-\infty})|_{z=0}$  is positive, which  
489 shows that a negative PVA must exist below the outcropping region for jets  
490 (if  $(\zeta_z + f_z)$  remains positive). Opposite sign generalised PVA is necessarily  
491 associated with opposite sign PVA gradients and to instability (Charney  
492 and Stern, 1962). Similarly to isolated vortices, integral constraint 36 can  
493 be useful to study the instability of surface fronts and for methods aiming at  
494 reconstructing the ocean at mesoscale and submesoscale via an estimation  
495 of PVA within the water column (Lapeyre et al., 2006; Ponte et al., 2013;  
496 Spall, 1995; Boss et al., 1996; Manucharyan and Timmermans, 2013).

#### 497 5.4. PV modification by bottom boundary layer processes

498 To study the modification of PV by -necessarily- diabatic processes, Eq.  
499 4 complemented with the knowledge of diabatic terms is needed (Benthuy-  
500 sen and Thomas, 2012; Molemaker et al., 2015; Gula et al., 2015, 2019).  
501 However, as shown next, integral constraints may provide an interesting  
502 way to monitor the PV evolution within an isopycnic layer intersecting the  
503 topography.

504 To do so let us consider the development of a bottom boundary layer in  
505 2D, with no variation in the  $y$  direction (Fig. 7).



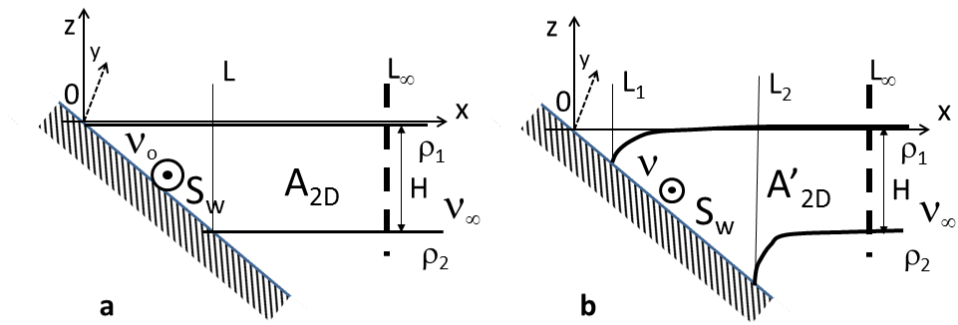


Figure 7: Vertical density structures in the deep ocean, near a topography. We consider a 2D configuration and we follow the evolution of a layer determined by two isopycnic levels  $\rho_1$  and  $\rho_2$  intersecting the topography. The initial velocity profile and the positions of the isopycnic levels (a) are modified by some diabatic processes (b).

506 We also consider that there is no outcropping at the surface and we fol-  
 507 low a control area  $A_{2D}$  bounded by two isopycnic surfaces  $\rho_1$  and  $\rho_2$ , the  
 508 topography and a vertical boundary located at a distance  $L_\infty$  sufficiently  
 509 large so that we can consider being away from the boundary layer and un-  
 510 affected by the diabatic processes (the stratification and velocity field are  
 511 unchanged, see Fig. 7). Integration of PV over this area gives (see Eq. 35):

$$\int \int_{A_{2D}} PV_{Ertel} dA = \left[ \int_{S^w} (\rho_1 - \rho_b) \vec{n} \cdot d\vec{l} + \int_{S^{\rho_2}} (\rho_1 - \rho_2) \vec{n} \cdot d\vec{l} \right] \cdot \vec{f} \\ - \int_{S^w} (\vec{U} \times \vec{\nabla} \rho) \cdot \vec{n} \cdot d\vec{l} - \int_{S^\infty} \mathcal{V}_\infty \partial_z \rho_\infty dz \quad (37)$$

512 Given its definition, the last term in Eq. 37 does not vary.

513 The isopycnic levels initially intersect the topography at  $x = 0$  and  
 514  $x = L$ , and along the topography the velocity field is  $\mathcal{V}_o \vec{j}$  (Fig. 7a). After  
 515 some diabatic processes, involving the viscous boundary layer and diapycnal  
 516 mixing, the velocity profile and the position of isopycnic surfaces are modi-  
 517 fied. The positions of the intersection with the topography are now  $x = L_1$   
 518 and  $x = L_2$  and the velocity field along the topography is  $\mathcal{V} \vec{j}$  (Fig. 7b).  
 519 Some trivial manipulations give:

$$\int_{S^w} (\rho_1 - \rho_b) \vec{n} \cdot d\vec{l} = -f_z \int_{L_1}^{L_2} (\rho_1 - \rho_b) dx \\ \int_{S^{\rho_2}} (\rho_1 - \rho_2) \vec{n} \cdot d\vec{l} = f_z (\rho_2 - \rho_1) (L_\infty - L_2) \\ - \int_{S^w} (\vec{U} \times \vec{\nabla} \rho) \cdot \vec{n} \cdot d\vec{l} = - \int_{\rho_1}^{\rho_2} \mathcal{V} d\rho \quad (38)$$

520 Assuming a linear variation of the density along the bottom topography,  
 521 this gives for the initial condition (see Fig. 7):

$$\int \int_{A_{2D}} PV_{Ertel} dA = f_z (\rho_2 - \rho_1) (L_\infty - \frac{L}{2}) - \overline{V}_o (\rho_2 - \rho_1) - \int_{S_\infty} \mathcal{V}_\infty \partial_z \rho_\infty dz \quad (39)$$

522 and after the diabatic modification:

$$\int \int_{A'_{2D}} PV_{Ertel} dA = f_z (\rho_2 - \rho_1) (L_\infty - \frac{L_1 + L_2}{2}) - \overline{V} (\rho_2 - \rho_1) - \int_{S_\infty} \mathcal{V}_\infty \partial_z \rho_\infty dz \quad (40)$$

523 where  $\overline{V}$  is the mean velocity along the bottom topography (where the av-  
 524 erage is weighted by density). The net modification of the volume integral  
 525 of PV within the layer is thus:

$$\Delta \int \int_{layer} PV = -(\rho_2 - \rho_1) f_z \Delta X_{bot}^{\rho_1/\rho_2} - (\rho_2 - \rho_1) \Delta \mathcal{V}_{bot}^{\rho_1/\rho_2} \quad (41)$$

526 where  $\Delta \mathcal{V}_{bot}^{\rho_1/\rho_2} = \overline{V} - \overline{V}_o$  is the modification of the mean velocity field along  
 527 the bottom and within the layer  $\rho_1/\rho_2$ , and  $\Delta X_{bot}^{\rho_1/\rho_2} = \frac{(L_1+L_2)-L}{2}$  is the  
 528 modification of the mean  $x$  position of the layer along the bottom.

529 If no-slip conditions are chosen at the bottom, we recover that only  
 530 density mixing along the bottom can modify the volume integral of PV  
 531 within a layer, as already discussed in section 4.4. The time evolution of the  
 532 volume integral of PV then only depends on the variation of the position  
 533 of the intersection of the isopycnic layer: it is negative if the layer goes  
 534 downslope (destratification case as illustrated in Fig. 7) and positive if  
 535 the layer goes upslope (restratification case). Our results are qualitatively  
 536 consistent with Benthuisen and Thomas (2012), despite the fact that we  
 537 consider a layer and not a fixed box for the volume integral of PV.

538 Equation 41 allows the possibility to consider free-slip bottom condi-  
 539 tions. Free-slip boundary conditions is the constraint usually used in nu-  
 540 merical models and can provide an additional modification of the volume  
 541 integral of PV if viscous effects are considered, as first imagined by D’Asaro  
 542 (1988). These viscous effects have to be added to the effect of the modifi-  
 543 cation of density studied in Benthuisen and Thomas (2012) and discussed  
 544 above. Equation 41 shows that they superimpose when calculating the vol-  
 545 ume integral of PV and generally act similarly. Since our results are only  
 546 diagnostics, we have to ”imagine” the evolution of the velocity and density  
 547 fields along the boundary to evaluate the possible PV modification. If we  
 548 consider a velocity field with the shallow region on its right ( $\overline{\mathcal{V}}_o < 0$ , as de-  
 549 picted in Fig. 7), in the northern hemisphere, the bottom friction develops  
 550 a downslope Ekman flux that leads to destratification and mixing induces a  
 551 negative volume integral of PV variation. We can also assume that bottom  
 552 friction also acts so as to reduce the strength of the velocity along the bot-  
 553 tom topography, so that  $|\overline{\mathcal{V}}| < |\overline{\mathcal{V}}_o|$ . This leads to  $\Delta \mathcal{V}_{bot}^{\rho_1/\rho_2} > 0$  and again to  
 554 a negative volume integral of PV variation. Similarly an initial current with  
 555 shallow region on its left would lead to a positive variation. This is consis-  
 556 tent with recent high resolution numerical results, using free-slip boundary  
 557 conditions (see Molemaker et al., 2015; Gula et al., 2015; Vic et al., 2015;  
 558 Gula et al., 2016, 2019) .

559 However, as discussed above, the important dynamical quantity is not  
 560 necessarily the volume integral of PV. The key quantity is the PVA within  
 561 an isopycnic layer. We can diagnose the mean PVA evolution within the  
 562 boundary layer by dividing the volume integral of PV by the volume of  
 563 the followed fluid (or its area  $A_{2D}$  and  $A'_{2D}$  in 2D, see Fig. 7). When  
 564 all isopycnic surfaces remain parallel, this volume is constant (as is the

565 case in Benthuisen and Thomas, 2012, for instance), the mean PVA is  
566 similar to the volume integral of PV and all previous results thus apply  
567 to the mean PVA. However, when this is not the case, the modification of  
568 PVA is more complex and also involves PV dilution or concentration within  
569 a layer which respectively gains or loses mass (see Haynes and McIntyre,  
570 1990; Morel and McWilliams, 2001). This process is effective whenever  
571 there exists variation of turbulence along the topography, which is the case  
572 if the bottom slope or the velocity field vary spatially. In addition, global  
573 mass conservation requires that the depletion of one layer coincides with  
574 the inflation of another layer. Thus, differential diapycnal mixing in bottom  
575 boundary layers is probably ubiquitous in realistic configurations and we  
576 can expect the creation of both positive and negative PV anomalies.

## 577 **6. Summary and discussion**

### 578 *6.1. Summary*

579 In the present paper, we have used three different formulations of Ertel  
580 PV in divergence form (see Schneider et al., 2003, and Eq. 9) to calculate a  
581 volume integral of PV from the knowledge of physical fields at the surface  
582 encompassing the volume. The divergence form and associated integral con-  
583 straints have then been used to enable easier calculation of PV for numerical  
584 models, also preserving the balances between boundary conditions and PV.  
585 This has been explored in more details for specific physical processes at  
586 different scales.

587 We have also shown that the integral constraints associated with the  
588 divergence form lead to an easier calculation of the PV expression for non  
589 Cartesian coordinate systems. We have in particular illustrated this by

590 calculating its expression in isopycnal coordinates for the general Navier-  
591 Stokes equations.

592 We have then considered the volume integral of PV within a "layer"  
593 delimited by two isopycnic surfaces and their intersections with the ocean  
594 surface and bottom. A general integral constraint was derived which allows  
595 to extend the PV impermeability theorem to no-slip conditions provided  
596 there is no density mixing along the topography. The integral constraint is  
597 then applied to several specific processes.

598 We first explored the link between volume integral of PV and surface  
599 fields at basin scale and we proposed an indicator to evaluate the time  
600 evolution of the volume integral of PV within a layer provided it outcrops  
601 at the sea surface (section 5.1). We proposed an indicator  $I_{surf}$ , depending  
602 on physical fields at the surface, as the signature of deeper PV. The indicator  
603 can be easily calculated for models and compared to observations (it depends  
604 on physical fields that can be estimated using satellite observations: wind,  
605 sea surface height, surface temperature and salinity).

606 When applied to isolated vortices or jets, given the equivalence between  
607 outcropping and surface PVA concentration (Bretherton, 1966), the balances  
608 indicate that such structures have opposite sign generalised PVA and are  
609 thus potentially unstable. It also provides a useful constraint to estimate  
610 PVA structures from surface information as currently attempted empirically  
611 (Lapeyre et al., 2006; Lapeyre and Klein, 2006; Lapeyre, 2009; Ponte et al.,  
612 2013; Wang et al., 2013; Fresnay et al., 2018).

613 We finally applied the integral constraints to the modification of PV  
614 by diabatic processes within the bottom boundary layer. This provides a  
615 diagnostic of the PV evolution within a layer based on the displacement of its  
616 mean position and on the modification of the mean along slope velocity along

617 the topography. It shows in particular that free-slip boundary conditions  
618 have potentially stronger effects on the formation of PVA in the viscous  
619 boundary layer. Differential mixing (variation of the density mixing along  
620 the topography) also leads to additional and possibly opposite sign PVA  
621 along the topography.

## 622 *6.2. Discussion*

623 Concerning the calculation of PV in numerical models, the divergence  
624 form approach can be adapted to any type of grid (including unstructured  
625 grids). In numerical models, the main problem is however Lagrangian con-  
626 servation of PV during the (adiabatic) evolution of the flow. This principally  
627 relies on numerical schemes used in the model. There exists debates on the  
628 optimality of numerical grids (for instance between the Charney-Phillips grid  
629 and the 3D C-grid, see Arakawa and Moorthi, 1988; Bell, 2003) but a fair  
630 comparison relies on comparable numerical schemes too: numerical schemes  
631 have to be optimised for the conservation of PV for each grid (see Winther  
632 et al., 2007). When this is established, the influence of the PV diagnostic  
633 on the conservation property is interesting to assess too, even though this  
634 influence is expected to be marginal compared to numerical schemes.

635 Concerning the  $I_{surf}$  indicator, we hypothesised that the time evolution  
636 of the integral of PV in a layer was mostly induced by the evolution of  
637 the surface fields. Recent studies (Ferrari et al., 2016; McDougall and Fer-  
638 rari, 2017; de Lavergne et al., 2017; Callies and Ferrari, 2018) have however  
639 shown that mixing is bottom intensified at large scale and that it is as-  
640 sociated with strong upwelling/downwelling circulations along the bottom  
641 topography which control the abyssal circulation overturning. According to  
642 what is discussed here in section 5.4, this can also modify the average PV.

643 The signature of the modification of the deep PV on surface and bottom  
644 boundary terms of the PV balance (Eq. 21) can be tested using numerical  
645 models (Deremble et al., 2014). Equation 14 can be used to calculate PV  
646 consistently with Eq. 21.

647 An interesting perspective is to combine the present results with the wa-  
648 ter mass transformation (WMT) approach (Walin, 1982; Tziperman, 1986;  
649 Speer and Tziperman, 1992). If the surface contribution to the volume in-  
650 tegral of PV can be exactly estimated for numerical models, we have to rely  
651 on geostrophic and Ekman currents for observations, so that we may miss  
652 some important ageostrophic contributions to the surface current, in partic-  
653 ular associated with mixing. The WMT theory allows one to estimate the  
654 surface drift associated with mixing and heat fluxes and correct the surface  
655 observations where needed. The importance of this term for the PV balance  
656 can be assessed in models and the WMT approach provides a way to take  
657 this effect into account in observations.

658 Concerning the dynamics of isolated vortices and jets, the balances can  
659 be easily extended to take into account variations of density along the bot-  
660 tom (variations of bottom density have then to be included in Eq. 34 and  
661 36) and a variable stratification at rest (see Eq. B.6 in Appendix B). This  
662 implies that the PVA evaluation is also possibly influenced by the bottom  
663 conditions, so that it may be difficult to reconstruct PVA profiles from the  
664 knowledge of surface density anomalies alone. Our calculations used the  
665 f-plane approximation. On the  $\beta$ -plane, weak vortices are dispersed into  
666 Rossby waves and their initial isolated nature can be rapidly lost. The re-  
667 sults we derive here are thus of interest mainly for coherent vortices whose  
668 PV structures is comprised of closed PV contours. For these vortices, we  
669 can neglect the variation of the Coriolis parameter and Rossby waves.



670 Concerning modification of PV in the bottom boundary layer, the net  
671 modification of PV is also a function of time (Benthuisen and Thomas,  
672 2013): the velocity and stratification in the bottom boundary layer do not  
673 reach instantaneously their equilibrium value (Benthuisen and Thomas,  
674 2012). Thus, the final modification of PV along a boundary depends on  
675 the time a fluid parcel will remain in contact with the boundary layer. A  
676 Lagrangian perspective shows that 3D effects are important for realistic  
677 conditions: when a circulation encounters a bottom boundary, a fluid parcel  
678 will be in contact with the boundary layer for a limited time period which  
679 is a function of the boundary and circulation shapes (see Fig. 8). Both  
680 frictional effects and diapycnal mixing will modify the PV value of the fluid  
681 parcel and the strength of the created PVA which eventually separates from  
682 the boundary.

683 The identified processes for PV modification in the bottom boundary  
684 layer have physical grounds but their implementation in numerical simula-  
685 tions is a delicate issue as the result also depends on the choices of several  
686 parameters (turbulent viscosity and diffusion, but also numerical schemes,  
687 boundary conditions and closure schemes for momentum and tracers in the  
688 bottom boundary layer). Further studies are needed to evaluate the respec-  
689 tive strength of each process in numerical simulations and in nature. The  
690 present results give exact diagnostics that can be helpful for that purpose.

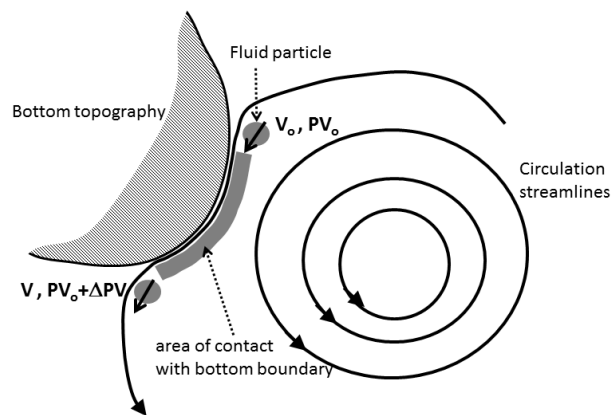


Figure 8: Schematic view of the modification of the PV of a fluid parcel that enters and exits a bottom boundary layer. The PV modification is a function of the time period the parcel remains within the bottom boundary layer, which is itself a function of the circulation and topography characteristics.

691 **Appendix A. General mathematical properties**

692 For the sake of application to PV, we name  $\vec{U}$ ,  $\vec{\zeta}$  and  $\rho$  the fields used  
 693 in the following equations, but the latter are exact general mathematical  
 694 results whatever the meaning of the  $\vec{U}$ ,  $\vec{\zeta}$  and  $\rho$  fields.

695 First let us recall some basic properties for the divergence and curl of  
 696 arbitrary fields:

$$\text{div}(\vec{U} \times \vec{B}) = (\vec{\nabla} \times \vec{U}) \cdot \vec{B} - (\vec{\nabla} \times \vec{B}) \cdot \vec{U}, \quad (\text{A.1a})$$

$$\text{div}(\rho \vec{\zeta}) = \vec{\zeta} \cdot \vec{\nabla} \rho + \rho \text{div}(\vec{\zeta}), \quad (\text{A.1b})$$

$$\vec{\nabla} \times (\rho \vec{U}) = \rho (\vec{\nabla} \times \vec{U}) - \vec{U} \times \vec{\nabla} \rho, \quad (\text{A.1c})$$

$$\text{div}(\vec{\nabla} \times \vec{U}) = 0, \quad (\text{A.1d})$$

$$\vec{\nabla} \times (\vec{\nabla} \rho) = \vec{0}. \quad (\text{A.1e})$$

697

698 Using  $\vec{U} = \vec{U}_a$  and  $\vec{B} = \vec{\nabla} \rho$  in A.1a, and  $\vec{\zeta} = \vec{\nabla} \times \vec{U}_a$  in A.1b, Eq. A.1  
 699 allow to derive the divergence forms of the PV (Eq. 9).

700 We also use the Ostrogradsky-Stokes theorems for the integration of  
 701 divergence and curl fields:

$$\int \int \int_V \text{div}(\vec{A}) dV = \int \int_{\partial V} \vec{A} \cdot d\vec{S} \quad (\text{A.2})$$

and

$$\int \int_S (\vec{\nabla} \times \vec{A}) \cdot d\vec{S} = \int_{\partial S} \vec{A} \cdot d\vec{l} \quad (\text{A.3})$$

702 where  $V$  is a finite volume,  $\partial V$  is its external surface and  $d\vec{S}$  is an elementary  
 703 surface oriented outward and is perpendicular to  $\partial\Omega$ ,  $S$  is a surface,  $\partial S$  is

704 its boundary and  $d\vec{l}$  is an elementary line oriented parallel to  $\partial S$  and in the  
 705 trigonometric direction when  $S$  is "seen from above" (see Fig. A.9).

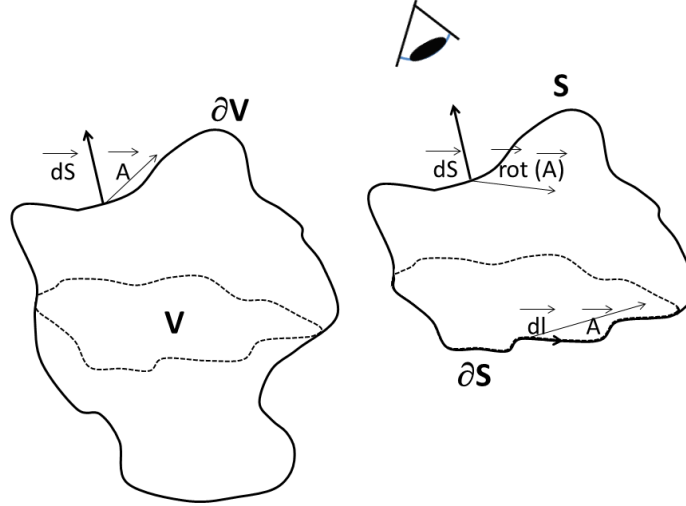


Figure A.9: Vector directions for the calculation of volume to surface to line integrals (Stokes theorem).

706 Finally, Eq. A.1 and A.3 also give:

$$\int \int_S \rho (\vec{\nabla} \times \vec{U}) \cdot d\vec{S} = \int \int_S (\vec{U} \times \vec{\nabla} \rho) \cdot d\vec{S} + \int_{\partial S} \rho \vec{U} \cdot d\vec{l}. \quad (\text{A.4})$$

707 All these integral properties allow the derivation of Eq. 10 and its alter-  
 708 native forms.

## 709 Appendix B. Generalised constraints in nonuniform stratification

### 710 Appendix B.1. Generalised PV

711 The definition of PV (Eq. 2) could be changed and  $\rho$  can be replaced  
 712 by  $G(\rho)$  where  $G$  represents a general function. The generalised PV form is

713 thus:

$$\begin{aligned}
PV_{Ertel-gen} &= -(\vec{\nabla} \times \vec{U} + \vec{f}) \cdot \vec{\nabla} G(\rho) \\
&= G'(\rho) PV_{Ertel}
\end{aligned} \tag{B.1}$$

714 and such a change does not alter the basic properties associated with PV  
715 and discussed in the paper.

716 The integral of the generalised Ertel PV satisfies all results discussed  
717 above. In particular, Eq. 10 becomes:

$$\begin{aligned}
\int \int \int_V PV_{Ertel-gen} dV &= - \int \int_{\partial V} G(\rho) (\vec{\nabla} \times \vec{U}_a) \cdot d\vec{S} \\
&= - \int \int_{\partial V} (\vec{U}_a \times \vec{\nabla} G(\rho)) \cdot d\vec{S} \\
&= - \int \int_{\partial V} G(\rho) \vec{f} \cdot d\vec{S} - \int \int_{\partial V} (\vec{U} \times \vec{\nabla} G(\rho)) \cdot d\vec{S}
\end{aligned} \tag{B.2}$$

718 The integration within a layer (Eq. 21) gives:

$$\begin{aligned}
\int \int \int_V PV_{Ertel-gen} dV &= [ \int \int_{S^s} (G(\rho_1) - G(\rho_s)) d\vec{S} \\
&\quad + \int \int_{S^b+S^w} (G(\rho_1) - G(\rho_b)) d\vec{S} \\
&\quad + \int \int_{S^{\rho_2}} (G(\rho_1) - G(\rho_2)) d\vec{S} ] \cdot \vec{f} \\
&\quad - \int \int_{S^s+S^b+S^w} (\vec{U} \times \vec{\nabla} G(\rho)) \cdot d\vec{S}
\end{aligned} \tag{B.3}$$

719 *Appendix B.2. Potential Vorticity Anomaly*

720 For a fluid at rest, where the velocity field and vorticity are null and the  
721 stratification only depends on the vertical coordinate, the previous gener-  
722 alised form gives:

$$\begin{aligned}
PV_{Ertel-gen}^{rest} &= -G'(\bar{\rho}) f_z \partial_z \bar{\rho} \\
&= -f_z \partial_z [ G(\bar{\rho}(z)) ]
\end{aligned}
\tag{B.4}$$

723 where  $f_z$  is the local vertical component of the Coriolis vector and  $\bar{\rho}(z)$  is  
724 the reference profile of the stratification at rest. Choosing  $G(X) = \bar{\rho}^{-1}(X)$ ,  
725 where  $\bar{\rho}^{-1}$  is the inverse of the function  $\bar{\rho}(z)$  (so that  $G(\bar{\rho}(z)) = z$ ), yields  
726  $PV_{Ertel-gen}^{rest} = -f_z$ : the reference PV is spatially uniform (f-plane approxi-  
727 mation).

728 Using the generalised form of PV given in Eq. B.1 and B.4, we calculate  
729 the generalised PVA:

$$\begin{aligned}
PVA_{gen} &= PV_{Ertel-gen} - PV_{Ertel-gen}^{rest} \\
&= -(\vec{\nabla} \times \vec{U} + \vec{f}) \cdot \vec{\nabla} G(\rho) + f_z
\end{aligned}
\tag{B.5}$$

730 Since the stratification at rest is constant, the calculation performed in  
731 section 5.2 can be reproduced to lead to the general integral constraints for  
732 isolated vortices in a nonuniform stratification:

$$\int \int \int PVA_{gen} dV + \int \int_{S^s} (G(\rho) - G(\rho_s^\infty)) (\zeta + f_z) dx dy = 0
\tag{B.6}$$

733 Note that  $G = \bar{\rho}^{-1}$  is a monotonically increasing function, so that all  
734 the physics discussed in section 5.2 remains qualitatively valid.

### 735 Acknowledgements

736 Yves Morel is supported by the program "IDEX attractivity chairs"  
737 from Université de Toulouse (TEASAO project) and CNES (french space

738 agency; project TOSCA/OSTST "Alti-ETAO"). This work also benefited  
739 from the Copernicus Marine Environment Monitoring Service (CMEMS)  
740 DIMUP project. CMEMS is implemented by Mercator Ocean in the frame-  
741 work of a delegation agreement with the European Union. J. Gula benefited  
742 support from LEFE/IMAGO through the Project AO2017-994457-RADII.  
743 A. Ponte benefited support from CNES for his participation to the SWOT  
744 Science Team (project "New Dynamical Tools"). The authors acknowledge  
745 discussions with Prof. Peter Haynes (Chair holder of the TEASAO project)  
746 and Drs. Leif Thomas, Jef Polton and John Taylor which helped improving  
747 this manuscript. This work has been drastically improved thanks to the crit-  
748 icisms, comments and careful reading of anonymous reviewers and of Ocean  
749 Modelling editors. Their encouragements have also been a strong support  
750 for us and their suggestions led to a far better presentation of our results.

## 751 **Bibliography**

- 752 Abernathey, R. P., Marshall, J., 2013. Global surface eddy diffusivities de-  
753 rived from satellite altimetry. *J. Geophys. Res.: Oceans* 118 (2), 901–916.
- 754 Arakawa, A., Lamb, V., 1977. Computational design of the basic dynamical  
755 processes of the ucla general circulation model. *Methods Comput. Phys.*  
756 17, 174–267.
- 757 Arakawa, A., Moorthi, S., 1988. Baroclinic instability in vertically discrete  
758 systems. *J. Atmos. Sci.* 45, 1688–1707.
- 759 Assassi, C., Morel, Y., Vandermeirsch, F., Chaigneau, A., Pegliasco, C.,  
760 Morrow, R., Colas, F., Fleury, S., Carton, X., Klein, P., Cambra, R.,

761 2016. An index to distinguish surface and subsurface intensified vortices  
762 from surface observations. *J. Phys. Oceanogr.* 46, 2529–2552.

763 Bell, M. J., 2003. Conservation of potential vorticity on lorenz grids. *Mon.*  
764 *Weather Rev.* 131 (7), 1498–1501.

765 Benthuisen, J., Thomas, L., 2012. Friction and diapycnal mixing at a slope:  
766 Boundary control of potential vorticity. *J. Phys. Oceanogr.* 42, 1509–1523.

767 Benthuisen, J., Thomas, L., 2013. Nonlinear stratified spindown over a  
768 slope. *J. Fluid Mech.* 726, 371–403.

769 Bleck, R., Rooth, C., Hu, D., Smith, L., 1992. Salinity driven thermocline  
770 transients in a wind and thermohaline forced isopycnic coordinate model  
771 of the North Atlantic. *J. Phys. Oceanogr.* 22, 1486–1505.

772 Boss, E., Paldor, N., Thompson, L., 1996. Stability of a potential vorticity  
773 front; from quasi-geostrophy to shallow-water. *J. Fluid Mech.* 315, 65–84.

774 Bretherton, C., Schar, C., 1993. Flux of potential vorticity substance: A  
775 simple derivation and a uniqueness property. *J. Atmos. Sci.* 50 (12), 1834–  
776 1836.

777 Bretherton, F., 1966. Critical layer instability in baroclinic flows. *Q.J.R.*  
778 *Meteorol. Soc.* 92 (2), 325–334.

779 Callies, J., Ferrari, R., 2018. Dynamics of an abyssal circulation driven by  
780 bottom-intensified mixing on slopes. *J. Phys. Oceanogr.*

781 Capet, X., McWilliams, J. C., Molemaker, M. J., Shchepetkin, A. F.,  
782 2008. Mesoscale to submesoscale transition in the California Current sys-



783 tem. part i: Flow structure, eddy flux, and observational tests. *J. Phys.*  
784 *Oceanogr.* 38 (1), 29–43.

785 Capet, X., Roulet, G., Klein, P., Maze, G., 2016. Intensification of upper-  
786 Ocean submesoscale turbulence through charney baroclinic instability. *J.*  
787 *Phys. Oceanogr.* 46 (11), 3365–3384.

788 Charney, J., Stern, M., 1962. On the stability of internal baroclinic jets in  
789 a rotating atmosphere. *J. Atmos. Sci.* 19 (2), 159–172.

790 Chelton, D. B., Schlax, M. G., Samelson, R. M., 2011. Global observations  
791 of nonlinear mesoscale eddies. *Progress in Oceanography* 91 (2), 167 –  
792 216.

793 Cushman-Roisin, B., Beckers, J.-M., 2011. *Introduction to Geophysical*  
794 *Fluid Dynamics*. Academic press, 875 pp.

795 Czaja, A., Hausmann, U., 2009. Observations of entry and exit of potential  
796 vorticity at the sea surface. *J. Phys. Oceanogr.* 39, 2280–2294.

797 D’Asaro, E., 1988. Generation of submesoscale vortices: A new mechanism.  
798 *J. Geophys. Res.:Oceans* 93-C6, 2156–2202.

799 Davis, C. A., Emanuel, K. A., 1991. Potential vorticity diagnostics of cyclo-  
800 genesis. *Mon. Weather Rev.* 119 (8), 1929–1953.

801 de Lavergne, C., Madec, G., Roquet, F., Holmes, R. M., McDougall, T. J.,  
802 2017. Abyssal Ocean overturning shaped by seafloor distribution. *Nature*  
803 551, 181.

804 Deremble, B., Wienders, N., Dewar, W. K., 2014. Potential vorticity budgets  
805 in the North Atlantic Ocean. *J. Phys. Oceanogr.* 44 (1), 164–178.

- 806 Ertel, H., 1942. On hydrodynamic eddy theorems. *Physikalische Zeitschrift*  
807 43, 526–529.
- 808 Ferrari, R., Mashayek, A., McDougall, T. J., Nikurashin, M., Campin, J.-  
809 M., 2016. Turning Ocean mixing upside down. *J. Phys. Oceanogr.* 46 (7),  
810 2239–2261.
- 811 Fresnay, S., Ponte, A. L., Le Gentil, S., Le Sommer, J., 2018. Reconstruction  
812 of the 3-d dynamics from surface variables in a high-resolution simulation  
813 of North atlantic. *J. Geophys. Res.: Oceans* 123 (3), 1612–1630.
- 814 Giordani, H., Lebeaupin Brossier, C., Léger, F., Caniaux, G., 2017. A  
815 pv-approach for dense water formation along fronts: Application to the  
816 Northwestern mediterranean. *J. Geophys. Res.: Oceans* 122 (2), 995–1015.  
817 URL <http://dx.doi.org/10.1002/2016JC012019>
- 818 Gula, J., Blacic, T. M., Todd, R. E., 2019. Submesoscale Coherent Vortices  
819 in the Gulf Stream. *Geophys. Res. Lett.* 46.
- 820 Gula, J., Molemaker, M., McWilliams, J., 2015. Topographic vorticity gen-  
821 eration, submesoscale instability and vortex street formation in the Gulf  
822 Stream. *Geophys. Res. Lett.* 42, 4054–4062.
- 823 Gula, J., Molemaker, M., McWilliams, J., 2016. Topographic generation of  
824 submesoscale centrifugal instability and energy dissipation. *Nature Com-*  
825 *munications* 7, 12811.
- 826 Hallberg, R., 1997. Stable split time stepping schemes for large-scale Ocean  
827 modeling. *J. Comp. Phys.* 135, 54–65.
- 828 Hallberg, R., Rhines, P., 1996. Buoyancy-driven circulation in an Ocean

829 basin with isopycnals intersecting the sloping boundary. *J. Phys.*  
830 *Oceanogr.* 26 (6), 913–940.

831 Hallberg, R., Rhines, P., 2000. Boundary sources of potential vorticity in  
832 geophysical circulations. *Developments in Geophysical Turbulence*, R. M.  
833 Kerr and Y. Kimura, Eds., Kluwer Academic, 51–65.

834 Haynes, P., McIntyre, M., 1987. On the evolution of vorticity and potential  
835 vorticity in the presence of diabatic heating and frictional or other forces.  
836 *J. Atmos. Sci.* 44 (5), 828–841.

837 Haynes, P., McIntyre, M., 1990. On the conservation and impermeability  
838 theorems for potential vorticity. *J. Atmos. Sci.* 47 (16), 2021–2031.

839 Held, I., Pierrehumbert, R., Garner, S., Swanson, K., 1995. Surface quasi-  
840 geostrophic dynamics. *J. Fluid Mech.* 282, 1–20.

841 Herbette, S., Morel, Y., Arhan, M., 2003. Erosion of a surface vortex by a  
842 seamount. *J. Phys. Oceanogr.* 33, 1664–1679.

843 Herbette, S., Morel, Y., Arhan, M., Nov. 2005. Erosion of a surface vortex  
844 by a seamount on the beta plane. *J. Phys. Oceanogr.* 35 (11), 2012–2030.

845 Holland, W. R., Keffer, T., Rhines, P., 1984. Dynamics of the Oceanic  
846 general circulation: The potential vorticity field. *Nature* 308, 698–705.

847 Holliday, D., McIntyre, M. E., 1981. On potential energy density in an in-  
848 compressible, stratified fluid. *J. Fluid Mech.* 107, 221–225.

849 Hoskins, B. J., McIntyre, M. E., Robertson, A. W., 1985. On the use and  
850 significance of isentropic potential vorticity maps. *Q. J. Roy. Met. Soc.*  
851 470, 877–946.

- 852 Kang, D., Fringer, O., 2010. On the calculation of available potential energy  
853 in internal wave fields. *J. Phys. Oceanogr.* 40 (11), 2539–2545.
- 854 Klein, P., Hua, B. L., Lapeyre, G., Capet, X., Gentil, S. L., Sasaki, H.,  
855 2008. Upper Ocean turbulence from high-resolution 3d simulations. *J.*  
856 *Phys. Oceanogr.* 38 (8), 1748–1763.
- 857 Lapeyre, G., 2009. What vertical mode does the altimeter reflect? on the  
858 decomposition in baroclinic modes and on a surface-trapped mode. *J.*  
859 *Phys. Oceanogr.* 39 (11), 2857–2874.
- 860 Lapeyre, G., 2017. Surface quasi-geostrophy. *Fluids* 2 (1).
- 861 Lapeyre, G., Klein, P., 2006. Dynamics of the upper Oceanic layers in terms  
862 of surface quasigeostrophy theory. *J. Phys. Oceanogr.* 36, 165–176.
- 863 Lapeyre, G., Klein, P., Hua, B., 2006. Oceanic restratification forced by  
864 surface frontogenesis. *J. Phys. Oceanogr.* 36 (8), 1577–1590.
- 865 Luyten, J. R., Pedlosky, J., Stommel, H., 1983. The ventilated thermocline.  
866 *J. Phys. Oceanogr.* 13 (2), 292–309.
- 867 Manucharyan, G., Timmermans, M.-L., 2013. Generation and separation of  
868 mesoscale eddies from surface Ocean fronts. *J. Phys. Oceanogr.* 43 (12),  
869 2545–2562.
- 870 Marshall, J., Nurser, G., 1992. Fluid dynamics of Ocean ic thermocline  
871 ventilation. *J. Phys. Oceanogr.* 22, 583–595.
- 872 McDougall, T. J., Ferrari, R., 2017. Abyssal upwelling and downwelling  
873 driven by near-boundary mixing. *J. Phys. Oceanogr.* 47 (2), 261–283.

- 874 McIntyre, M. E., Norton, W., 2000. Potential vorticity inversion on a hemi-  
875 sphere. *J. Atmos. Sci.* 57, 1214–1235.
- 876 McWilliams, J., 2006. *Fundamentals of Geophysical Fluid Dynamics*. Cam-  
877 bridge University Press.
- 878 McWilliams, J., Flierl, G., 1979. Evolution of isolated, non-linear vortices.  
879 *J. Phys. Oceanogr.* 9 (6), 1155–1182.
- 880 McWilliams, J. C., 1984. The emergence of isolated coherent vortices in  
881 turbulent flow. *J. Fluid Mech.* 146, 21–43.
- 882 Meunier, T., Rossi, V., Morel, Y., Carton, X., 2010. Influence of bottom to-  
883 pography on an upwelling current: Generation of long trapped filaments.  
884 *Ocean Modell.* 41, 277–303.
- 885 Molemaker, M. J., McWilliams, J. C., Dewar, W. K., 2015. Submesoscale  
886 instability and generation of mesoscale anticyclones near a separation of  
887 the California Undercurrent. *J. Phys. Oceanogr.* 45 (3), 613–629.
- 888 Morel, Y., Darr, D., Talandier, C., 2006. Possible sources driving the po-  
889 tential vorticity structure and long-wave instability of coastal upwelling  
890 and downwelling currents. *J. Phys. Ocean.* 36, 875–896.
- 891 Morel, Y., McWilliams, J., May 1997. Evolution of isolated interior vortices  
892 in the Ocean. *J. Phys. Ocean.* 27 (5), 727–748.
- 893 Morel, Y., McWilliams, J., 2001. Effects of isopycnal and diapycnal mixing  
894 on the stability of Ocean ic currents. *J. Phys. Ocean.* 31, 2280–2296.
- 895 Morel, Y., Thomas, L., 2009. Ekman drift and vortical structures. *Ocean*  
896 *Modell.* 27, 185–197.

- 897 Pedlosky, J., 1987. *Geophys. Fluid Dyn.* Springer, New York, 710 pp.
- 898 Polton, J., Marshall, D., 2003. Understanding the structure of the subtrop-  
899 ical thermocline. *J. Phys. Oceanogr.* 33 (6), 1240–1249.
- 900 Ponte, A., Klein, P., Capet, X., Traon, P. L., Chapron, B., Lherminier, P.,  
901 2013. Diagnosing surface mixed layer dynamics from high-resolution satel-  
902 lite observations: Numerical insights. *J. Phys. Oceanogr.* 43 (7), 1345–  
903 1355.
- 904 Rhines, P., 1986. Vorticity dynamics of the Ocean ic general circulation.  
905 *Annual review of Fluid Mechanics* 18, 433–497.
- 906 Rhines, P., Young, W., 1982a. Homogenization of potential vorticity in plan-  
907 etary gyres. *J. Fluid Mech.* 122, 347–367.
- 908 Rhines, P., Young, W., 1982b. A theory of the wind-driven circulation. i,  
909 mid-Ocean gyres. *J. Mar. Res.* 40, 559–596.
- 910 Rio, M., Mulet, S., Picot, N., 2014. Beyond GOCE for the Ocean circula-  
911 tion estimate: Synergetic use of altimetry, gravimetry, and in situ data  
912 provides new insight into geostrophic and ekman currents. *Geophys. Res.*  
913 *Lett.* 41 (24), 8918–8925.
- 914 Ripa, P., 1991. General stability conditions for a multi-layer model. *J. Fluid*  
915 *Mech.* 222, 119–137.
- 916 Rossi, V., Morel, Y., Garcon, V., 2010. Effect of the wind on the shelf dy-  
917 namics: formation of a secondary upwelling along the continental margin.  
918 *Ocean Modell.* 31, 51–79.

- 919 Roulet, G., McWilliams, J. C., Capet, X., Molemaker, M. J., 2012. Proper-  
920 ties of steady geostrophic turbulence with isopycnal outcropping. *J. Phys.*  
921 *Oceanogr.* 42 (1), 18–38.
- 922 Schneider, T., Held, I., Garner, S., 2003. Boundary effects in potential vor-  
923 ticity dynamics. *J. Atmos. Sci.* 60 (8), 1024–1040.
- 924 Spall, M., 1995. Frontogenesis, subduction, and cross-front exchange at up-  
925 per Ocean fronts. *J. Geophys. Res.* 100, 2543–2557.
- 926 Speer, K., Tziperman, E., 1992. Rates of water mass formation in the North  
927 Atlantic Ocean. *J. Phys. Oceanogr.* 22 (1), 93–104.
- 928 Sudre, J., Morrow, R. A., 2008. Global surface currents: a high-resolution  
929 product for investigating Ocean dynamics. *Ocean Dynamics* 58 (2), 101.
- 930 Sutyrin, G., Flierl, G., 1994. Intense vortex motion on the beta-plane -  
931 Development of the beta-gyres. *J. Atmos. Sci.* 51 (5), 773–790.
- 932 Talley, L. D., 1988. Potential vorticity distribution in the North Pacific. *J.*  
933 *Phys. Oceanogr.* 18 (1), 89–106.
- 934 Taylor, J., Ferrari, R., 2010. Buoyancy and wind-driven convection at mixed  
935 layer density fronts. *J. Phys. Oceanogr.* 40, 1222–1242.
- 936 Thomas, L., Ferrari, R., 2008. Friction, frontogenesis, and the stratification  
937 of the surface mixed layer. *J. Phys. Oceanogr.* 38 (11), 2501–2518.
- 938 Thomas, L., Rhines, P., 2002. Nonlinear stratified spin-up. *J. Fluid Mech.*  
939 473, 211–244.
- 940 Thomas, L., Taylor, J., Ferrari, R., 2013. Symmetric instability in the Gulf  
941 Stream. *Deep-Sea Res.* 91, 96–110.

- 942 Thomas, L. N., 2005. Destruction of potential vorticity by winds. *J. Phys.*  
943 *Oceanogr.* 35 (12), 2457–2466.
- 944 Tziperman, E., 1986. On the role of interior mixing and air-sea fluxes in  
945 determining the stratification and circulation of the Ocean s. *J. Phys.*  
946 *Oceanogr.* 16 (4), 680–693.
- 947 Vallis, G. K., 2006. *Atmospheric and Oceanic Fluid Dynamics*. Cambridge  
948 University Press, Cambridge, U.K.
- 949 Vic, C., Roulet, G., Capet, X., Carton, X., Molemaker, M. J., Gula, J.,  
950 2015. Eddy-topography interactions and the fate of the Persian Gulf Out-  
951 flow. *J. Geophys. Res.: Oceans* 120 (10), 6700–6717.  
952 URL <http://dx.doi.org/10.1002/2015JC011033>
- 953 Walin, G., 1982. On the relation between sea-surface heat flow and thermal  
954 circulation in the Ocean. *Tellus* 34 (2), 187–195.
- 955 Wang, J., Flierl, G. R., LaCasce, J. H., McClean, J. L., Mahadevan, A.,  
956 2013. Reconstructing the Ocean ’s interior from surface data. *J. Phys.*  
957 *Oceanogr.* 43 (8), 1611–1626.
- 958 Wenegrat, J. O., Thomas, L. N., Gula, J., McWilliams, J. C., 2018. Effects of  
959 the submesoscale on the potential vorticity budget of Ocean Mode Waters.  
960 *J. Phys. Oceanogr.* 48 (9), 2141–2165.
- 961 White, A. A., Hoskins, B. J., Roulstone, I., Staniforth, A., 2005. Consistent  
962 approximate models of the global atmosphere: shallow, deep, hydrostatic,  
963 quasi-hydrostatic and non-hydrostatic. *Q. J. Roy. Met. Soc.* 131 (609),  
964 2081–2107.



965 Winther, N., Morel, Y., Evensen, G., 2007. Efficiency of high order numerical  
966 schemes for momentum advection. *J. Mar. Sys.* 67, 31–46.